Hindawi Publishing Corporation
ISRN Soil Science
Volume 2013, Article ID 424178, 33 pages
http://dx.doi.org/10.1155/2013/424178

Review Article

Remote Sensing of Soil Moisture

Venkat Lakshmi

Department of Earth and Ocean Sciences, University of South Carolina, Columbia, SC 29208, USA

Correspondence should be addressed to Venkat Lakshmi; vlakshmi@geol.sc.edu

Received 14 November 2012; Accepted 13 December 2012

Academic Editors: G. Benckiser, J. A. Entry, and Z. L. He

Soil moisture is an important variable in land surface hydrology as it controls the amount of water that infiltrates into the soil and replenishes the water table versus the amount that contributes to surface runoff and to channel flow. However observations of soil moisture at a point scale are very sparse and observing networks are expensive to maintain. Satellite sensors can observe large areas but the spatial resolution of these is dependent on microwave frequency, antenna dimensions, and height above the earth's surface. The higher the sensor, the lower the spatial resolution and at low elevations the spacecraft would use more fuel. Higher spatial resolution requires larger diameter antennas that in turn require more fuel to maintain in space. Given these competing issues most passive radiometers have spatial resolutions in 10s of kilometers that are too coarse for catchment hydrology applications. Most local applications require higher-spatial-resolution soil moisture data. Downscaling of the data requires ancillary data and model products, all of which are used here to develop high-spatial-resolution soil moisture for catchment applications in hydrology. In this paper the author will outline and explain the methodology for downscaling passive microwave estimation of soil moisture.

1. Introduction

Soil moisture is an important variable in land surface hydrology. Soil moisture has very important implications for agriculture, ecology, wildlife, and public health and is probably (after precipitation) the most important connection between the hydrological cycle and life—animal, plant, and human.

Land surface hydrology is a well-studied portion of the terrestrial water cycle. The main variables in land-surface hydrology are soil moisture, surface temperature, vegetation, precipitation, and streamflow. Of these, surface temperature, vegetation, and precipitation are currently observed using satellites, and streamflow is routinely observed at in situ watershed locations. Soil moisture remains the only variable not observed (or observed very sparsely) either in situ or via remote sensing. Due to this very reason, in the past decade, satellite soil moisture has been increasingly used in hydrological, agricultural, and ecological studies due to its spatial coverage, temporal continuity, and (now) easiness of use.

Numerous studies have shown the influence of soil moisture on the feedbacks between land-surface and climate that has a profound influence on the dynamics of the atmospheric boundary layer and a direct relationship to weather and global climate [1–4]. Chang and Wetzel [5] have shown the influence of spatial variations of soil moisture and vegetation on the development and intensity of severe storms, whereas Engman, 1997 [6], demonstrated the ability of soil moisture to influence surface moisture gradients and to partition incoming radiative energy into sensible and latent heat. In large-scale modeling, the soil moisture and surface temperature are key variables in deciding the depth of the planetary boundary layer and circulation and wind patterns [7–9]. It has been demonstrated that the assimilation of soil moisture observations in hydrologic models can improve the accuracy of estimated hydrological variables such as evaporation, surface temperature, and root-zone soil moisture [10–12]. The various atmospheric processes that affect the land surface and in turn the influence of the land surface on the atmosphere need to be clearly quantified. In order to accomplish these tasks, it is necessary to intimately understand the relationship of soil moisture to these phenomena on small and large spatial scales. Unfortunately we are limited in our ability to completely observe large-scale hydrologic land-surface interactions. Satellite and aircraft remote sensing enable us to

estimate large-scale soil moisture for the purpose of modeling the interactions between land and atmosphere, helping us to model weather and climate with higher accuracy.

Recognizing the need for soil moisture observations on large spatial scales for continental scale hydrological modeling investigators in the 1980s used the special sensor microwave Imager (SSM/I) [13] and scanning multichannel microwave radiometer [14] data sets. The SMMR data has been used to study soil moisture retrievals, sensitivity, and scaling on continental scales [15–17]. The SSM/I [15, 18] has been used in catchment scale studies [19] and in continental scale studies in conjunction with a hydrological model [20–22]. More recently, successful retrieval has been carried out using several missions including WindSat [23], tropical rainfall measuring mission (TRMM) microwave imager (TMI) [24]. Recently a promising soil moisture data set has been developed jointly by researchers of NASA Goddard Space Flight Center and the Vrije Universiteit Amsterdam [25]. It utilizes C-band AMSR-E microwave brightness temperatures in a Land Parameter Retrieval Model (LPRM) to obtain soil moisture. This product has been tested in a series of validation studies (e.g., [26–28]) and shows high correlations with field observations [29]. The Global Change Observation Mission-Water (GCOM-W) launched by the Japanese Space Agency is now providing us with microwave data sets of the land surface [30].

Active and passive microwave remote sensing provides a unique capability to obtain observations of soil moisture at global and regional scales that help satisfy the science and application needs for hydrology [31–33]. The emissive and scattering characteristics of soil surface depend on soil moisture among other variables, that is, surface temperature, surface roughness, and vegetation. The electromagnetic response of the land surface is modified by soil moisture and modulated by surface roughness, vegetation canopy effects, and interaction with the atmosphere before being received by a sensor. These ancillary (non-soil-moisture) effects increase at higher frequencies making low-frequency observations desirable for observation of soil moisture [34, 35]. Longer wavelengths also sense deeper soil layers (2–5 cm) at the L-band, the penetration depth being of the order of one tenth of the wavelength [36]. Retrieval of soil moisture using ground-based or aircraft-mounted radiometer operating at the L-band has been demonstrated in several prior studies [37–42].

An important experiment for investigating the capability of the PALS (passive and active L-and S-bands radiometer/radar) was conducted in the Southern Great Plains region of United States in July 1999. The SGP99 experiments included bare, pasture, and agricultural crop surface cover with field averaged vegetation water contents mainly in the 0–2.5 kg m^{-2} range. Studies based on the SGP99 experiments exhibited varying soil moisture retrieval potential, with a 2-3% accuracy using passive channels and 2–5% accuracy using the active channels of the PALS instrument [40, 42]. There was a need to conduct similar studies under higher vegetation water contents in order to evaluate the performance of soil moisture retrieval algorithms under these conditions.

The Soil Moisture Experiments in 2002, SMEX02 were conducted in Iowa over a one-month period between mid-June and mid-July, 2002. A major focus of SMEX02 was extension of instrument observations and algorithms to more challenging vegetation conditions and understanding the implications on soil moisture retrieval. In situ measurements of gravimetric soil moisture, soil temperature, soil bulk density, and vegetation water content were carried out coincidently with PALS observations in active and passive channels. This study evaluated the performance of existing algorithms and models for soil moisture retrieval using active and passive measurements under the moderately high to very high vegetation water content conditions.

Field scale validation networks exist in Oklahoma [43–45], Illinois [46], and the USDA operational SCAN (Soil Climate Analysis Network) [47]. Soil observing networks have their challenges especially when used to validate satellite data sets [48].

The NASA soil moisture active passive (SMAP) mission [53], is set for launch in 2014. SMAP will utilize a very large antenna and combined radiometer/radar measurements to provide soil moisture at higher resolutions than radiometers alone can currently achieve. SMAP [53] consists of both passive and active microwave sensors. The passive radiometer will have a nominal spatial resolution of 36 km and the active radar will have a resolution of 1 km. The active microwave remote sensing data can provide a higher spatial resolution observation of backscatter than those obtained from a radiometer (order of magnitude: radiometer ~40 km and radar ~1 km or better). Radar data are more strongly affected by local roughness, microscale topography, and vegetation than a radiometer, meaning that it is difficult to invert backscatter to soil moisture accurately, thus limiting the development of such algorithms. Therefore, it can be difficult to use radar data alone. SMAP will use high-resolution radar observations to disaggregate coarse resolution radiometer observations to produce a soil moisture product at 3 km resolution. The soil moisture has been retrieved from radiometer data successfully using various sensors and platforms and these retrieval algorithms have an established heritage [31, 54].

There have been methods integrating the use of active sensors that have a higher spatial resolution to downscale passive microwave soil moisture retrievals [55–57]. Recent studies have addressed the soil moisture downscaling problem using MODIS sensor derived temperature, vegetation, and other surface ground variables. The major publications in this area of study include the following. (i) A method based on a "universal triangle" concept was used to retrieve soil moisture from Normalized Difference Vegetation Index (NDVI) and land surface temperature (LST) data [50]. (ii) A relationship between fractional vegetation cover and soil evaporative efficiency was explored for catchment studies in Southeastern Australia by Merlin et al., 2010 [49] while Merlin et al., 2008 [51], developed a simple method to downscale soil moisture by using two soil moisture indexes: evaporative fraction (EF) and the actual EF (AEF) [58]. (iii) A sequential model which used MODIS as well as ASTER (Advanced Scanning Thermal Emission and Reflection Radiometer) data

Table 1: Studies on downscaling soil moisture using various remote sensing and modeling techniques [41].

Author	Methodology	Time and region	Result
Merlin et al., [49]	Based on the relationship between soil evaporative efficiency and soil moisture	NAFE 2006 (Oct-Nov), Yanco, Southeastern Australia	Mean correlation slope between simulated and measured data is 0.94, the most accuracy with an error of 0.012
Piles et al., [50]	Build model between LST, NDVI, and soil moisture	Jan-Feb 2010, Murrumbidgee catchment, Yanco, Southeastern Australia	R^2 is between 0.14~0.21 and RMSE 0.9~0.17
Merlin et al., [51]	Downscaling algorithm is derived from MODIS and physical-based soil evaporative efficiency model	NAFE 2006 (Oct-Nov), Murrumbidgee catchment, Yanco, Southeastern Australia	Overall RMSE is between 1.4%~1.8% v/v
Merlin et al., [51]	Based on two soil moisture indices EF and AEF	June and August 1990 (Monsoon' 90 experiment), USDA-ARS WGEW in southeastern Arizona	Total accuracy is 3% vol. for EF and 2% vol. for AEF, and correlation coefficient is 0.66~0.79 for EF and 0.71~0.81 for AEF
Merlin et al., [52]	Sequential model	NAFE 2006 (Oct-Nov), Yanco, Southeastern Australia	RMSE is −0.062 vol./vol. and the bias is 0.045 vol./vol.

was proposed for downscaling soil moisture [52, 59, 60]. Table 1 lists these studies, the methods, and significant results of the soil moisture downscaling.

This paper is organized as follows. Section 2 outlines the theory of passive microwave radiative transfer. Section 3 explains results from the Soil Moisture Experiment 2002 (SMEX02) using aircraft-based passive and active sensors. Section 4 describes two methods used for disaggregation of soil moisture: (1) use of active sensors to detect change in soil moisture at a finer scale and use that information for construction of higher spatial resolution estimates of soil moisture and (2) use of visible and near infrared satellite observations to disaggregate passive microwave satellite soil moistures. Section 5 discusses the future of remote sensing of soil moisture.

2. The Radiative Transfer Model

The earth's surface as seen by a spaceborne or airborne radiometer may include bare or vegetated soil, varying amounts of roughness, similar or varying soil types, and variation in the soil moisture content.

Any model of radiative transfer from the earth's surface must incorporate the effects of these factors observed brightness temperatures. The radiative transfer model described here begins with the bare soil emissivity and then is modified for roughness and vegetation. Most of the studies using the model have been done in the 1.4–6.6 GHz range. Atmospheric effects on the brightness temperatures and the effects of volume scattering are not considered, as they are negligible at these frequencies (1.4–6.6 GHz).

2.1. Emissivity of a Smooth Surface. The relationship between the brightness temperature T_B of a radiating body and its thermodynamic temperature T_s is given by the expression

$$T_B = eT_s, \tag{1}$$

where e is the emissivity of the body T_B expressed in Kelvins. The emissivity is related to the reflectivity r of the surface by

$$e = 1 - r. \tag{2}$$

For a smooth surface and a medium of uniform dielectric constant, the expressions for reflectivity at horizontal and vertical polarizations may be derived from electromagnetic theory [1] as

$$r_v = \left| \frac{\varepsilon_r \cos\theta - \sqrt{\varepsilon_r - \sin^2\theta}}{\varepsilon_r \cos\theta + \sqrt{\varepsilon_r - \sin^2\theta}} \right|^2,$$
$$r_h = \left| \frac{\cos\theta - \sqrt{\varepsilon_r - \sin^2\theta}}{\cos\theta + \sqrt{\varepsilon_r - \sin^2\theta}} \right|^2, \tag{3}$$

where θ is the incidence angle and ε_r is the complex dielectric constant of the medium.

2.2. Emissivity of a Bare Smooth Soil. Water has a much higher dielectric constant compared to soil. An increase in the soil water content increases both the real and imaginary parts of the dielectric constant of the soil-water mix. The dielectric properties of wet soils have been studied by several

investigators [61, 62] (e.g., [63, 64]). The texture of the soil also plays an important role in determining its dielectric constant. The dielectric constant for wet soil is evaluated using an empirical mixing model from Fang et al. [61]. For the purposes of this study the moisture content of the soil is assumed to be uniform to the penetration depth of the sensor and the effects of nonuniformity of moisture with depth are not considered.

2.3. Effect of Surface Roughness. Surface roughness causes the emissivity of natural surfaces to be somewhat higher [1, 35, 65, 66]. This is attributed mainly to the increased surface area of the emitting surface. A semiempirical expression for rough surface reflectivity from Ni-Meister et al. [12] is used to account for surface roughness:

$$r_p = \left[Qr_{0q} + (1-Q)\, r_{0p}\right] \exp(-h), \tag{4}$$

where r_{0q} and r_{0p} are the reflectivities the medium would have if the surface were smooth. The expression utilizes two parameters, which are dependent on the surface conditions. Q is the polarization mixing parameter and h is the height parameter. These two parameters depend on the frequency, look angle of the sensor, and the roughness of the surface and have to be determined experimentally.

The values of Q and h are useful for fitting and modeling experimental data, but recent theoretical calculations have indicated that Q and h are not directly related to the parameters, rms height, and horizontal correlation length, measured in the field and used to characterize rough surface reflectivity [67].

2.4. Effect of Vegetation. The presence of vegetation canopy in natural areas and crop canopy in agricultural fields has a significant effect on the remotely sensed microwave emission from soils [68, 69]. The sensitivity of measured microwave emission in vegetation-covered fields will be different from bare fields. Vegetation is modeled as a single homogenous layer above the soil. The brightness temperature T_B^p corresponding to polarization p, vertical (v), or horizontal (h) over such a dual vegetation-soil layer is given by Das et al. [57]:

$$T_B^p = e_p T_s \exp(-\tau) + T_C\left[1-\exp(-\tau)\right]\left[1 + r_p \exp(-\tau)\right], \tag{5}$$

where T_C is the vegetation temperature, T_s is the soil temperature, τ is the vegetation opacity, and e_p and r_p are the soil emissivity and reflectivity, respectively. The value of τ is dependent on frequency, vegetation type, and vegetation water content. The relationship between τ and the vegetation water content W_e can be described by the following equation from [16, 35]:

$$r = \frac{bW_e}{\cos\theta}, \tag{6}$$

where b is a function of canopy type, polarization, and wavelength and $\cos\theta$ accounts for the nonvertical/slant path through the vegetation.

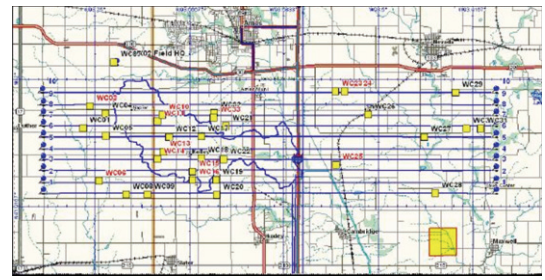

Figure 1: The Walnut Creek watershed region and PALS flight lines are shown by the blue lines [41].

The land surface as seen by the satellite sensor is a heterogeneous combination of vegetated and bare areas. The vegetated and bare areas have to be disaggregated to find the proportion of the radiation that reaches the sensor from the different types of land cover. The land surface can be disaggregated into a completely shadowed fraction M and a bare soil fraction M by utilizing the leaf area index (LAI). Leaf area index (LAI) defines an important structural property of a plant canopy, the number of equivalent layers of leaves the vegetation possesses relative to a unit ground area:

$$M = 1 - e^{-\mu \mathrm{LAI}}, \tag{7}$$

where μ is the extinction coefficient. The proportion of microwave brightness temperatures contributed by bare soils and vegetated regions within a certain area can be calculated using

$$T_B = MT_B^{\mathrm{canopy}} + (1-M)\, T_B^{\mathrm{bare}}, \tag{8}$$

where T_B^{canopy} is from (5) and T_B^{bare} corresponds to brightness temperature of bare soil ((1) with emissivity corresponding to bare soil). This gives us ability to model microwave brightness temperatures that would be detected by a sensor.

3. Results from the SMEX02 Field Experiment

3.1. SMEX02 Experiment. The Soil Moisture Experiments in 2002 (SMEX02) were conducted in Iowa between June 25 and July 12th, 2002. The study site chosen was Walnut Creek, a small watershed in Iowa. This watershed has been studied extensively by the USDA and hence was well instrumented for in situ sampling of hydrologic parameters. The terrain is undulating and the land lover type for the watershed region is primarily agricultural with corn and soybeans being the major crops. Figure 1 shows a map of the study region indicating the location of the data collection sites and the layout of the aircraft flight lines. The experiments were conducted from 25 June to 12th July, 2002, during which the soybean fields grew from essentially bare soils to vegetation water content of 1–1.5 kg/m^2 while the corn fields grew from 2-3 kg/m^2 to 4-5 kg/m^2 (Figures 2 and 3). SMEX02 provided unique conditions of high initial biomass content and significant change in biomass over the course of the experiment. The fields selected for in situ sampling

Table 2: Sensitivity of radiometer channel to 0–6 cm layer gravimetric soil moisture evaluated over corn and soy fields, respectively. The LH channel has the maximum sensitivity with the sensitivity being much greater over soy fields than corn fields [41].

Period	LH	LV	SH	SV
		Corn		
176–178	−0.386	−0.242	−0.131	−0.076
186-187	−0.831	−0.284	−0.644	−0.070
187-188	−0.316	−0.165	−0.164	−0.124
188-189	−0.357	−0.132	−0.132	−0.084
		Soy		
176–178	−1.182	−0.333	0.183	−0.054
186-187	−1.013	−0.426	0.787	−0.425
187-188	−1.117	−0.409	−0.379	−0.133
188-189	−1.050	−0.848	−1.047	−0.665

Figure 2: Field WC05 on July 8 (VWC ~ 4.8 kg/m^2) [41].

Figure 3: Field WC03 on July 8 (VWC ~ 0.85 kg/m^2) [41].

were approximately 800 m × 800 m and the sampling points were distributed throughout the field to take into account the variations in soil types and therefore soil moisture within each field.

The PALS instrument was flown over the SMEX02 region on June 25, 27 and July 1st, 2nd, 5, 6, 7, and 8, 2002 (corresponding to DOY 176, 178, 182, 183, 186, 187, 188, and 189, resp.). Initial soil conditions were dry but scattered thunderstorms occurred between July 4 and 6 enabling a wetting and subsequent dry down to be observed. The PALS radiometer and radar provided simultaneous observations of horizontally and vertically polarized L- and S-bands brightness temperatures, radar backscatter measured in VV, HH and VH configurations, and nadir-looking thermal infrared surface temperature. The instrument was flown on a C-130 (velocity ~ 70 m/s) aircraft at a nominal altitude of ~3500 feet with the angle of incidence on the surface being ~45 degrees. In this configuration the instantaneous 3 dB footprint on the surface was 330 m × 470 m. The instrument thus sampled a single line footprint track along the flight path. Aircraft location and navigation data and downward looking thermal infrared (IR) temperatures were also recorded in addition to the radiometer and radar measurements.

3.2. Sensitivity. Sensitivity for the passive sensor is evaluated as the ratio of the change in emissivity to the change in gravimetric soil moisture $\Delta e/\Delta m_g$ and as the change in radar backscatter to the change in percentage gravimetric soil moisture $\Delta\sigma/\Delta(m_g\%)$ for the active sensor. The estimation of emissivity was carried out by dividing the brightness temperature in a channel by the surface temperature. Sensitivity of the radiometer is expected to be negative as an increase in soil moisture results in a decrease in the emissivity while the sensitivity of the radar is supposed to be positive as the value of backscatter increases with increase in soil moisture. Overlying vegetation tends to attenuate the radiometric response of soil thereby reducing sensitivity of the microwave sensor to soil moisture, the effect of which is seen in the reduced sensitivity over corn fields as compared to soy fields. Some of the sensitivity values presented in the study have positive values for radiometer channels and negative values for radar channels indicating that overlying vegetation completely mask sout the effect of soil moisture on observed brightness temperatures and backscatter coefficients. These measures of sensitivity allow an intercomparison between different channels of the radar or the radiometer.

There was major precipitation event in the watershed region on July 7 which provided around 24 mm of rain on the SMEX02 study region. Sensitivity computation was done by averaging PALS observations in a particular channel for corn and soy fields separately and comparing the change in averaged PALS observations to the change in the 0–6 cm layer soil moisture before and after the precipitation event. The results have been presented in Tables 2 and 3. As expected, the L band horizontal polarization channel had the maximum sensitivity among passive channels with a maximum sensitivity of 0.831 over corn fields and 1.182 over soy fields. For the radar channels the L band vertically copolarized backscatter was most sensitive to soil moisture with sensitivities of 0.421 for corn and 0.639 for soy fields. The S-band was less sensitive to soil moisture than the L band with the maximum sensitivities for passive and active PALS observations being 0.644 (SH) and 0.12 (SVV) over corn fields and 1.047 (SH) and 0.380 (SVV) over soy fields. These findings illustrate the lower capability of the S-band to penetrate denser vegetation canopies as in case of corn fields as opposed to soybean fields which had significantly lower vegetation water content. In general, the PALS sensor exhibited greater sensitivity over the less vegetated soy fields

Table 3: Sensitivity of radar channel to 0–6 cm layer gravimetric soil moisture evaluated over corn and soy fields. L band vertically copolarized channel is seen to be most sensitive to soil moisture and the sensitivity is seen to be higher for soy fields as compared to corn fields. A number of negative sensitivity values during the dry period DOY 176–178 indicate that the contribution of soil moisture to the radar backscatter was masked out by vegetation and surface roughness effects [41].

Period	lhh	lvv	lvh	shh	svv	svh
			Corn			
176–178	0.237	0.115	−0.214	0.138	−0.173	0.051
187-188	0.222	0.302	0.199	0.114	0.120	0.122
188-189	0.309	0.421	0.374	0.078	0.103	0.113
			Soy			
176–178	0.019	−0.114	0.329	−0.001	−0.521	−0.086
187-188	0.454	0.639	0.360	0.387	0.380	0.324
188-189	0.625	0.504	0.666	0.335	0.105	0.219

Active channels (sensitivity = $(\Delta\sigma/\Delta m_g) * 0.01$).

Table 4: Correlations between PALS horizontal polarization brightness temperatures and soil moisture in the 0-1 cm and 0–6 cm layers. Correlations generally reduce with increasing vegetation water content. The 2.5 kg/m^2 < VWC < 3.5 kg/m^2 and 1.0 kg/m^2 < VWC < 2.5 kg/m^2 classes consist mostly of measurements made in the corn fields for the dry days of June 25th and 26th when the contribution of radiation from soil is masked out by the overlying vegetation and the coefficient of correlation is seen to be positive [41].

VWC (kg/m^2)	No. of points	GSM (0-1 cm)		GSM (0–6 cm)	
		R (LH)	R (SH)	R (LH)	R (SH)
VWC < 1.0	52	−0.881	−0.885	−0.808	−0.846
1.0 < VWC < 2.5	6	0.142	0.278	0.420	0.562
2.5 < VWC < 3.5	21	−0.094	−0.197	0.258	0.161
3.5 < VWC < 4.5	13	−0.950	−0.863	−0.847	−0.833
VWC > 4.5	48	−0.690	−0.641	−0.676	−0.626

(VWC ~ 1.0 Kg/m^2) in comparison to the cornfields (VWC ~ 3.5 Kg/m^2) across all channels. These findings support previous studies showing the LH channel to be more sensitive to near-surface soil moisture than LV, SH, or SV and the LVV channel to be more sensitive to soil moisture than other active channels [36].

3.3. Statistical Analysis. Numerous prior studies have focused on either regression between radiometer or radar observations and in situ observations of surface soil moisture [71, 72] under conditions of low vegetation water content. The relationship between soil moisture and microwave emission is nearly linear. The present study evaluates the performance of linear regression technique for soil moisture estimation under the conditions of high vegetation water content encountered during the SMEX02 campaign.

Soil moisture retrieval was carried out by a simple multilinear regression procedure. As the best correlation between brightness temperatures and soil moisture was given by a band combination of LH, LV, and SH bands a multilinear regression was done using two combinations of PALS channels (LH, LV, and SH) and (LH, SH). Soil moisture retrieval was also carried out using the brightness temperatures from a single LH channel. Individual observations were classified into five subclasses depending on the vegetation water content. Table 4 presents the correlation coefficients (R) obtained from a linear regression applied to the colocated data for all available days of PALS observations. Significant correlation was seen between the L band horizontal polarization brightness temperature and in situ soil moisture for three of the subclasses with a negative value indicating that the brightness temperature decreases as soil moisture increases. Regression equations were developed for each class using 2-3 days of observations (calibration period) and the soil moisture was retrieved for all other days (validation period) using these (calibration) equations. Average root mean square error (RMSE) was computed for the soil moisture retrieval in each case. Tables 5 and 10 present the errors associated with retrieval of soil moisture from the LH band and the band combination LH, LV, and SH. The retrieval errors reduce significantly when multichannel regression retrieval is done, especially in the case of the highest vegetation water content class (VWC > 4.5) where the lowest retrieval error of 0.045 g/g (gravimetric soil moisture) is obtained for the band combination LH, LV, and SH as compared to 0.062 g/g for retrieval from the LH band only. Similarly, retrieval error for the class with VWC < 1 kg/m^2 is also the least in case of LH, LV, and SV band combination, the error being 0.034 g/g. As expected the retrieval accuracies decrease with increase in vegetation water content indicating that the sensor becomes less sensitive to soil moisture as the vegetation water content increases.

Retrieval of soil moisture was also done by employing linear or multiple regressions between the colocated radar

Table 5: Root mean square errors associated with soil moisture retrieval from the PALS LH channel by the statistical regression technique. Note that the retrieval errors are greatest for the VWC > 4.5 kg/m^2 class [41].

Calibration days	Note	VWC < 1.0	1 < VWC < 2.5	2.5 < VWC < 3.5	3.5 < VWC < 4.5	VWC > 4.5
178, 189	1 dry, 1 wet	0.0371	0.0326	0.0579	0.0417	0.0623
176, 186, 188	1 dry, 2 wet	0.0371	0.0302	0.0578	0.0409	0.0738
178, 188, 189	1 dry, 2 wet	0.0374	0.0322	0.0492	0.0410	0.0643
176, 178, 189	2 dry, 1 wet	0.0375	0.0271	0.0609	0.0417	0.0623
176, 178, 187	2 dry, 1 wet	0.0383	0.0328	0.0531	0.0450	0.0635
188, 189	2 wet	0.0403	0.0337	—	0.0402	0.0643
176, 178	2 dry	0.1459	0.1228	0.0774	—	—

Table 6: Correlations between PALS vertically copolarized radar backscatter and soil moisture in the 0-1 cm layer. Correlations generally reduce with increasing vegetation water content. The 1.0 kg/m^2 < VWC < 2.5 kg/m^2 and 2.5 kg/m^2 < VWC < 3.5 kg/m^2 classes consist mostly of measurements made in the corn fields for the dry days of June 25th and 26th when the contribution of radiation from soil is masked out by the overlying vegetation and the coefficient of correlation is seen to be negative [41].

VWC (kg/m^2)	No. of points	GSM (0-1 cm)		GSM (0–6 cm)	
		R (LVV)	R (SVV)	R (LVV)	R (SVV)
VWC < 1.0	57	0.858	0.814	0.79	0.73
1.0 < VWC < 2.5	8	0.443	0.222	0.17	0.389
2.5 < VWC < 3.5	28	−0.15	−0.146	−0.346	−0.434
3.5 < VWC < 4.5	14	0.742	0.794	0.457	0.482
VWC > 4.5	47	0.811	0.519	0.793	0.503

backscatter and in situ soil moisture dataset classified on the basis of vegetation water content. Table 6 presents the coefficient of correlation (R) values obtained by single channel linear regression for five different subclasses of vegetation water content. Active channels also give acceptable retrieval errors, with the lowest prediction error for the VWC > 4.55 kg/m^2 class being 0.0481 g/g for the LVV, SVV, and LHH band combination. The retrieval errors associated with soil moisture retrieval from PALS backscatter coefficients are tabulated in Tables 7 and 8.

It is important that the calibrating dataset fairly represents the conditions encountered during the course of the SMEX02 experiments. It is seen that the errors increase significantly if only dry or only wet days are used for calibration. Table 8 shows that the RMS error increases to 0.08 g/g from 0.05 g/g in case of fields with VWC between 2.5 and 3.5 kg/m^2, when 2 dry days were used for developing the regression equation rather than 1 dry 2 wet or 2 dry and 1 wet days. The discrepancy seen in the 2.5 kg/m^2 < VWC < 3.5 kg/m^2 and 1.0 kg/m^2 < VWC < 2.5 kg/m^2 classes in the form of a positive value of coefficient of correlation for the passive case and negative value for the active case (Tables 4 and 6) is due to the fact that these classes consist mostly of measurements made in the corn fields for the dry days of June 25 and 26 when the contribution of radiation from soil was masked out by the overlying vegetation. This effect is also reflected by the higher soil moisture retrieval errors for this class. Soil moisture retrieval by a multiple channel regression produces more prediction errors than single channel regression as the variance in both vegetation and soil moisture is taken into account by a multiple regression.

3.4. Forward Model for Passive Sensor. The forward model for simulation of brightness temperatures considers a uniform layer of vegetation overlying the soil surface. The dielectric behavior of the soil water mixture is modeled using a semiempirical, four-component, dielectric-mixing model [64]. The upwelling radiation from the land surface observed from above the canopy was expressed in terms of radiative brightness temperature and is described by the radiative transfer model [69, 73, 74].

A physical model for passive radiative transfer was used for simulation of PALS-observed brightness temperatures and subsequent soil moisture retrieval. In situ measurements of soil moisture, land surface temperature, bulk density, and vegetation water content were made during the SMEX02 experiments. The in situ measurements of vegetation water content were used to calibrate a model that used a Landsat TM derived parameter, NDWI, which was used to derive the vegetation water contents for the SMEX02 region for the entire study period. A summary of the parameters that were used for calibration and soil moisture retrieval from PALS-observed L band brightness temperatures has been presented in Table 9.

Soil surface roughness, h, polarization mixing parameter, q, and single scattering albedo were not available as measured quantities. Polarization mixing was taken as zero and single scattering albedo was taken as 0.1 for both vertical and horizontal polarizations for corn as well as soy canopies. Surface roughness was used as a free parameter for calibrating the model. Vegetation opacity was taken to be 0.086 for soy canopy and 0.12 for corn canopy as reported in previous studies [17]. For deriving the optimum values, h was varied between 0 and 0.6 separately for corn and soy fields and the estimation was done on the criteria of minimum root mean square error between PALS-observed average brightness temperature $(T_{BH} + T_{BV})/2$, in the L band and the modeled average brightness temperature for the L band. The average brightness temperatures were normalized by T_{LST} to account for surface temperature contribution. Calibration

Table 7: Root mean square errors associated with soil moisture retrieval from the PALS LVV, SVV, and LHH band combination. The errors generally increase with vegetation water content [41].

Calibration days	Note	VWC < 1.0	1 < VWC < 2.5	2.5 < VWC < 3.5	3.5 < VWC < 4.5	VWC > 4.5
178, 189	1 dry, 1 wet	0.0401	0.0340	0.0477	0.0447	0.0490
176, 186, 189	1 dry, 2 wet	0.0373	0.0286	0.0576	0.0551	0.0501
178, 188, 189	1 dry, 2 wet	0.0395	0.0293	0.0502	0.0439	0.0481
176, 178, 189	2 dry, 1 wet	0.0398	0.0319	0.0493	0.0443	0.0490
176, 178, 187	2 dry, 1 wet	0.0382	0.0340	0.0465	0.0450	0.0987
188, 189	2 wet	0.0571	0.1747	—	0.0443	0.0481
176, 178	2 dry	0.0421	0.0598	0.0497	—	—

Table 8: Root mean square errors associated with soil moisture retrieval from the PALS LVV band by the statistical regression technique [41].

Calibration days	Note	VWC < 1.0	1 < VWC < 2.5	2.5 < VWC < 3.5	3.5 < VWC < 4.5	VWC > 4.5
178, 189	1 dry, 1 wet	0.0430	0.0360	0.0474	0.0517	0.0505
176, 186, 189	1 dry, 2 wet	0.0424	0.0348	0.0511	0.0454	0.0505
178, 188, 189	1 dry, 2 wet	0.0430	0.0360	0.0498	0.0511	0.0507
176, 178, 189	2 dry, 1 wet	0.0447	0.0375	0.0478	0.0517	0.0505
176, 178, 187	2 dry, 1 wet	0.0441	0.0419	0.0465	0.0485	0.0517
188, 189	2 wet	0.0485	0.0665	—	0.0761	0.0507
176, 178	2 dry	0.0637	0.0731	0.0474	—	—

Table 9: Summary of parameters input to the radiative transfer model for simulation of PALS brightness temperatures [41].

(a) Media and sensor parameters	
Vegetation:	
Single scattering albedo, ω	0.1
Opacity coefficient, b	0.086 (soy), 0.12 (corn)
Soil:	
Roughness coefficients, h (cm) and Q	h-calibrated $Q = 0$.
Bulk density (g cm^{-3})	in-situ
Sand and clay mass fractions, s and c	CONUS-SOIL dataset
Sensor:	
Viewing angle, θ (deg)	45
Frequency, f (GHz)	1.41, 2.69
Polarization	H, V
(b) Media variables	
Land surface:	
Surface soil moisture, m_v (g cm^{-3})	In-situ
Vegetation water content, w_c (kg m^{-2})	Landsat TM
Surface temperature, t (K)	In-situ

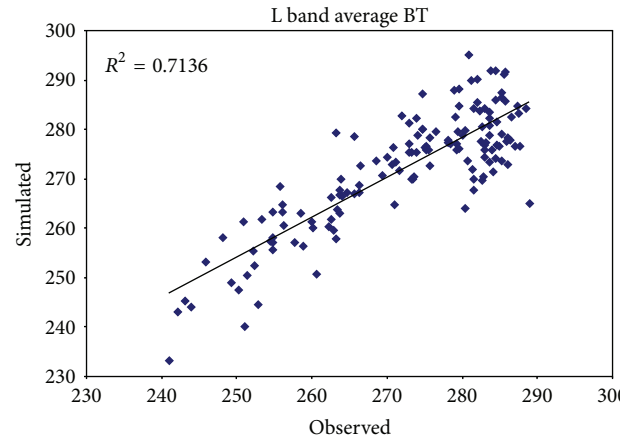

Figure 4: Model-predicted versus PALS-observed L band brightness average temperatures. The prediction is better at high soil moisture conditions (lower average brightness temperature) when contribution of vegetation and roughness is not as significant as that of soil moisture. Model calibrated using PALS and in situ data for July 7 and July 8 [41].

was performed for different combinations of 2 or 3 days of PALS observations out of the 7 days available.

The calibrated values of h for each field and in situ measurements of model soil moisture, bulk density, surface temperature, and vegetation water content were used to simulate horizontal and vertical polarization brightness temperatures for the L- and S-bands. Gravimetric soil moisture in the 0–6 cm layer was used. Simulations were run for various combinations of calibration days. The root mean square error (RMSE) for simulation of average brightness temperature in the L band was 7.1 K and 8.0 K for the S-band when the calibration was done for DOY's 176, 188, and 189. Simulation results were better for soy fields with an RMSE of 6.8 K as opposed to corn fields with an RMSE of 7.2 K for the L band. Figures 4 and 5 present the plots for PALS observed versus model-predicted average brightness temperature for the L- and S-bands. Retrieval of soil moisture was performed by using a simple retrieval algorithm that arrives at a soil moisture estimate by minimizing the error between simulated and observed L band average brightness temperature normalized with the land surface temperature

Table 10: Root mean square errors (g/g) associated with retrieval of soil moisture (gravimetric) by physical modeling of PALS L band observations considering the retrieved soil moisture is representative of the in situ 0–6 cm layer soil moisture [41].

Calibration days	Note	vwc < 1	1 < vwc < 2.5	2.5 < vwc < 3.5	3.5 < vwc < 4.5	4.5 < vwc
178, 189	1 dry, 1 wet	0.0375	0.0343	0.0287	0.0327	0.0439
176, 186, 189	1 dry, 2 wet	0.0404	0.0310	0.0365	0.0504	0.0436
178, 188, 189	1 dry, 2 wet	0.0475	0.0338	0.0309	0.0271	0.0398
176, 178, 189	2 dry, 1 wet	0.0398	0.0297	0.0230	0.0519	0.0518
176, 178, 187	2 dry, 1 wet	0.0442	0.0042	0.0252	0.0661	0.0465
188, 189	2 wet	0.0326	0.0341	0.0403	0.0334	0.0283
176, 178	2 dry	0.0455	0.0033	0.0221	0.0737	0.0472
176, 188, 189	1 dry, 2 wet	0.0333	0.0286	0.0299	0.0391	0.0454

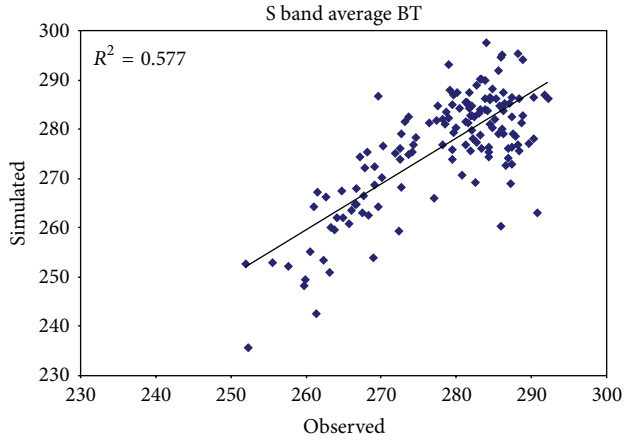

Figure 5: Model-predicted versus PALS-observed S-band average brightness temperatures. Model calibrated using PALS and in situ data for July 7 and July 8 [41].

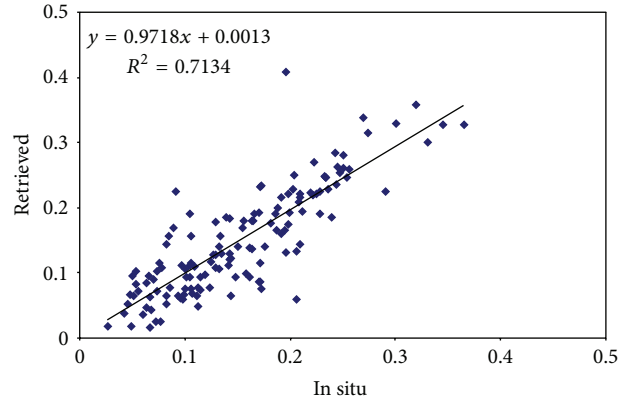

Figure 6: Model-retrieved gravimetric soil moisture (g/g) versus soil moisture measured in situ in the 0–6 cm soil layer. Model calibrated using PALS and in situ data for July 7 and July 8 [41].

(T_B(modeled) − T_B(observed)/T_{LST}), where T_{LST} is the land surface temperature in Kelvins. Soil moisture retrieval was done for various combinations of calibration days and the RMSE for the retrieval was evaluated in each case. Table 10 presents the errors between in situ soil moisture in the 0–6 cm soil layer and the model retrieved soil moisture values for five classes based on vegetation water content. The retrieval errors increase as the vegetation water content increases, being around 0.03 g/g for the VWC < 1 kg/m^2 fields and greater than 0.04 g/g for the fields with VWC > 4.5 kg/m^2. Figure 6 is a plot of soil moisture retrieved from PALS L band horizontal polarization brightness temperatures versus the in situ soil moisture in the 0–6 cm soil layer with the calibration being done using DOY's 176, 188, and 189.

Physical modeling of brightness temperatures proved to be more accurate than statistical regression technique with an overall soil moisture retrieval accuracy of around 0.036 g/g as compared to 0.05 g/g for the statistical regression technique. Error may have been introduced in the soil moisture retrieval process due to improper in-situ sampling, measurement of gravimetric soil moisture and bulk density and the assumption that single scattering albedo and vegetation opacity are independent of look angle and polarization. Assignment of a single value of h and q for all fields of a particular crop type is also a source of error and field measurements of surface roughness are desirable. In the present study both east-to-west and west-to-east flight lines were considered to maximize the number of fields observed by PALS on each day. If a field was observed during both the east-to-west and west-to-east passes, the value from the east-to-west flight line was chosen. This also introduces a source of error in both the statistical regression and physical modeling techniques of soil moisture retrieval as the PALS overpass times may not coincide with the in situ sampling time for soil moisture in a particular field, and data from two flight lines may be different due to factors such as sun glint.

4. Disaggregation of Soil Moisture

4.1. Radar-Radiometer Method

4.1.1. The Importance of Radar for Soil Moisture. Radars have a higher spatial resolution than radiometers. Retrieval of soil moisture using radar backscattering coefficients is difficult due to more complex signal target interaction associated with measured radar backscatter data, which is highly influenced by surface roughness and vegetation canopy structure and water content. Several empirical and semiempirical algorithms for retrieval of soil moisture from radar backscattering coefficients have been developed but they are valid mostly

in the low vegetation water content conditions [75–77]. On the other hand, the retrieval of soil moisture from radiometers is well established and has a better accuracy with limited requirements for ancillary data [78, 79]. Radiometer measurements are less sensitive to uncertainty in measurement and parameterization of surface roughness and vegetation canopy interaction. However, the spatial resolution of radiometer is much lower compared to radar operating in the same band. An optimal soil moisture retrieval algorithm that combines the higher spatial resolution of radar with higher sensitivity of a radiometer might result in improved soil moisture products.

Temporal evolution of soil moisture can be potentially monitored through change detection. Change detection methods [70] have been implemented as a convenient way to determine relative soil moisture or the change in soil moisture [42, 80]. Both brightness temperature and radar backscatter change depend approximately linearly on soil moisture and hence sensitivity can be assumed to be independent of soil moisture. However, quantification of sensitivity requires soil moisture measurements, which is difficult in the case of radar in the presence of moderate to high vegetation cover. It may be possible to estimate the radar sensitivity to soil moisture by using radiometer-estimated soil moisture measurements if the impact of vegetation on sensitivity and spatial heterogeneity issues can be accounted for.

This section proposes a simple algorithm that uses higher resolution radar observations along with coarser resolution radiometer observations to determine the change in soil moisture at the spatial resolution of radar operation, without using any in situ soil moisture measurements. The present study simplifies the problem of spatial disaggregation of soil moisture by considering that the spatial variability of bare soil properties (texture, roughness) that influence radar sensitivity to soil moisture is not significant and hence the variability of radar signal within the radiometer footprint is due to soil moisture and canopy vegetation water content variability only.

The next section explains the theoretical basis and assumptions behind the algorithm for spatial disaggregation used in this study. Section 4.1.3 presents the data and the methods that are applied to evaluate the performance of the algorithm presented in the study. Section 4.1.4 presents the results in terms of comparison of in situ measurements of soil moisture with the disaggregated estimates obtained from the algorithm.

4.1.2. Theory for Change Detection. Brightness temperature and radar backscatter have a nearly linear relationship to surface soil moisture, for uniform vegetation and land surface characteristics. The radiative transfer model for estimation of soil moisture from brightness temperature is well established and needs few ancillary parameters for soil moisture estimation. The C-band radiometer AMSR-E has a global soil moisture product and future L-band radiometers such as SMOS and HYDROS will have radiometer-only soil moisture products. However, the radiometer-only soil moisture product is limited in application by the low spatial resolution of the radiometer instrument. Higher spatial resolution is possible with radar soil moisture estimation; however, estimation of absolute soil moisture from radar backscattering coefficients requires modeling a complex signal target interaction. Even in empirical and semiempirical studies, vegetation canopy and soil parameters may be needed to classify a heterogeneous target area into subclasses that are fairly uniform in terms of those parameters. Several studies based on the approach of classification and linear parameterization of L-band radar backscatter measurements with respect to soil moisture within each class have been performed in the past [65, 76, 81, 82].

The approach taken by the present study is change estimation, which takes advantage of the approximately linear dependence of radar backscatter change on soil moisture change [42]. Njoku et al. demonstrated the feasibility of a change detection approach using the PALS radar and radiometer data obtained during the SGP99 campaign. The PALS and in situ soil moisture data were classified into 3 different classes based on the vegetation water content. For each class linear least square fits of PALS brightness temperature and radar backscatter to soil moisture were developed. The linear relationships were modeled as

$$T_{Bp} = A + Bm_v, \tag{9}$$

$$\sigma^0_{pp} = C + Dm_v. \tag{10}$$

The PALS data used for the SGP99 study had the same footprint size for both radar and radiometer. Hence, A, B, C, and D are parameters for each pixel in the coincident radar and radiometer images and were assumed to primarily be functions of surface vegetation and roughness (and temperature for the passive case). Difference images were obtained by subtracting the sensor data on the first day from the sensor data on the consecutive days. They were able to calibrate C and D parameters in (10) using 2 days of radiometer estimates of soil moisture under wet and dry soil conditions. Further using C, D, and σ^0_{vv} they derived radar-estimated soil moisture with satisfactory results. Our study is aimed at estimation of soil moisture change at the spatial resolution of radar by combining radar and radiometer data. The approach and assumptions are similar to the Njoku et al. study; however, in our case the radar is at higher spatial resolution of 100 m as compared to the 400 m spatial resolution of the radiometer. We assume that the changes in vegetation canopy parameters are insignificant as compared to the change in soil moisture when considering the resulting change in copolarized radar backscatter, given a sufficiently high revisit rate of the sensor over the target. Using this assumption, the difference image obtained by subtracting consecutive radar backscatter images acquired over an area would be given by

$$\Delta\sigma^0_{pp} = D\Delta m_v. \tag{11}$$

$\Delta\sigma^0_{pp}$ is the change in copolarized radar backscatter (dB) and Δm_v is the change in soil moisture. The parameter D is expected to depend on the attenuation characteristics of the

vegetation canopy and the surface roughness characteristics of the soil surface. Results from Friedl et al. [62] indicate that relative sensitivity of the L-band copolarized channels of radar should depend primarily on the vegetation canopy opacity. Relative sensitivity is defined as the ratio of the radar sensitivity in the presence of a vegetation canopy (D) to the sensitivity if there was only bare soil (D_0):

$$\frac{D}{D_0} = f(\tau). \tag{12}$$

Figure 12 in Du et al. shows the variation of the relative sensitivity for a medium rough soil surface having a soybean canopy. The plot suggests that relative sensitivity can be estimated from optical thickness once the canopy type and surface type are known. The vegetation opacity τ can be estimated using the ($\tau = b\text{VWC}/\cos\theta$) relationship for vegetation canopies that follow the electrically thin scatterer approximation. b is a parameter that depends on vegetation structure and type, θ is the incidence angle, and VWC is the vegetation water content which can be estimated operationally using proxies such as NDWI [83]. Now, combining (11) and (12) we can write

$$\Delta\sigma^0_{pp} = f(\tau)\, D_0 \Delta m_v. \tag{13}$$

The bare soil sensitivity D_0 depends only weakly on soil roughness variability for a given sensor configuration (frequency, polarization, and viewing angle). To substantiate this further, the author conducted a simulation in which the Integral Equation Model [65] was used to generate plots of vertically copolarized radar backscatter versus soil moisture for various root mean square soil roughness values (Figure 7). It is seen in the figure that the line plots for $s = 0.4$ cm to $s = 2.4$ cm can be approximated as a series of parallel lines with the same slope and different intercepts. The result indicates that for the L-band surface roughness variability has only a small effect on the soil moisture sensitivity of radar. Now, from (13) we obtain

$$\Delta m_v = \frac{\Delta\sigma^0}{S_0}, \tag{14}$$

where $S_0 = f(\tau) * D_0$. Let us assume that the radar backscatter is available at a finer resolution of "x" whereas radiometer data is available at a coarser resolution of "$\mathbf{X}$". The problem, then, is to estimate $\Delta m_{v,x}$, that is, the change in soil moisture from time step t_0 to $t_0 + \Delta t$, given $m_{v,\mathbf{X}}$, σ^0_x, and τ_x at times t_0 and $t_0 + \Delta t$ using (12). The change in the soil moisture at the coarser spatial resolution ($\mathbf{X}$) can be evaluated as the sum of all the changes at the finer resolution (x), that is,

$$\Delta m_{v,\mathbf{X}} = \frac{1}{N}\sum m_{v,x}. \tag{15}$$

The summation is over all the "N" smaller radar footprints within the larger radiometer footprint, and $\Delta m_{v,\mathbf{X}}$ is the change in soil moisture as measured by the radiometer at the lower spatial resolution, $\Delta m_{v,x}$ is the change in soil moisture as measured by the radar at the higher spatial resolution given by (12). Combining (12) and (13) leads to

$$\Delta m_{v,\mathbf{X}} = \frac{1}{N}\sum \frac{\Delta\sigma^0_x}{S_0}. \tag{16}$$

The unknown S_0 will be the same for all the radar pixels within a radiometer pixel given uniform vegetation characteristics within the radiometer footprint, that is, $f(\tau)$ is the same for all radar pixels within the radiometer pixels. The author recognize the fact that the spatial variability of $f(\tau)$ will not be low in a real world setting. However, in the case of the SMEX02 experiments, each radiometer footprint was contained completely within an agricultural field with fairly uniform vegetation characteristics. In the present study we do not attempt to model for the vegetation canopy variability within the radiometer footprint. S_0 is evaluated for each radiometer pixel by dividing the summation of change in radar backscattering coefficients with the change in radiometer scale soil moisture. The summation is for all radar pixels that lie within the radiometer pixel:

$$S_0 = \frac{1}{N}\frac{\sum \Delta\sigma^0_x}{\Delta m_{v,\mathbf{X}}}. \tag{17}$$

S_0 for a particular radiometer pixel can be resampled to the radar spatial resolution and for each radar pixel within the radiometer pixel we write the change in soil moisture at resolution "x" as

$$\Delta m_{v,x} = \frac{\Delta\sigma^0_x}{S_0}. \tag{18}$$

Another important issue in the low spatial variability of S_0 assumption is the implicit assumption that multiple days of radar data were obtained over the region at the same angle of incidence. At different incidence angles, corresponding AIRSAR pixels will exhibit different sensitivity to soil moisture. During SMEX02, the near and far look angles were 22.8° and 71.3° and July 5, 22.0° and 71.2° for July 7, and 24.1° and 71.3° for July 8. This indicates that AIRSAR acquired data over each of the fields at approximately similar incidence angles for the three days. The variation of incidence angles between two fields is not important as the relative change in radar backscatter is considered with the relative change in the soil moisture on a field-wise basis. The low-resolution sensitivity parameter S_0 is derived separately for each field. As a result only the variation of incidence angle within each field will be important and this variation is small. Within the dimensions of the PALS footprint, this variation in AIRSAR incident angles will be small and its effect on sensitivity negligible.

Accurate estimation of the change in soil moisture at the lower spatial resolution ($\Delta m_{v,\mathbf{X}}$) is crucial to the accuracy of computed radar sensitivity to soil moisture (15) and hence the accuracy of the high-resolution soil moisture change estimated by the approach presented in this paper. In an operational setting $\Delta m_{v,\mathbf{X}}$ can be estimated from single-or multichannel passive remote sensing observations. Estimation of soil moisture from passive remote sensing

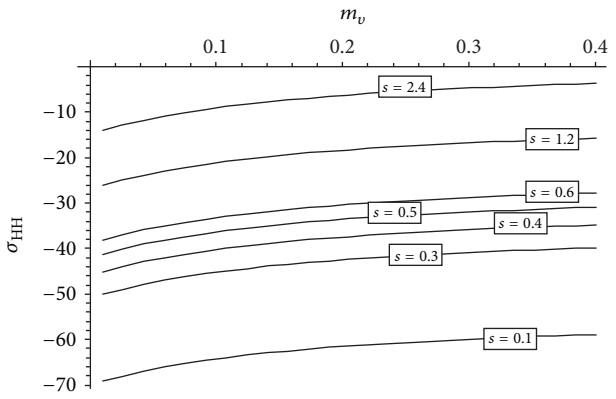

Figure 7: Simulation of L band horizontally copolarized radar backscattering coefficients using the integral equation model [70] for various values of volumetric soil moisture m_v and rms surface roughness s (cm). Surface correlation length has been taken as 8 cm, % sand = 30, and % clay = 30. For various roughness values, moisture versus backscatter curves can be approximated as straight lines with the same slope. L band vertically copolarized radar backscattering coefficients show a similar behaviour too [55].

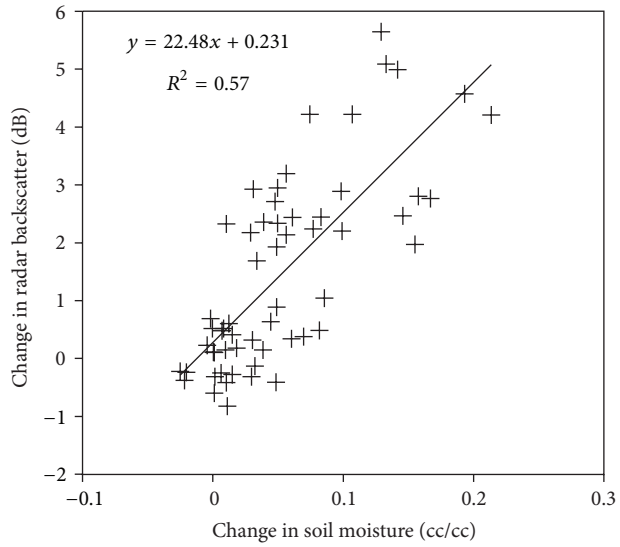

Figure 8: Plot of change in AIRSAR LVV backscatter at 800 m resolution versus change in in situ volumetric soil moisture at a 800 m resolution for the periods July 5 to July 7 and July 5 to July 8 [55].

has been studied in several prior works and the author do not attempt to retrieve soil moisture from PALS radiometer data used in this study. A previous study [41] demonstrated PALS radiometer to be sensitive to soil moisture during the SMEX02 experiments and retrieval of soil moisture from PALS L-band brightness temperature data was done with estimation errors of approximately 4%. In the current study, in situ soil moisture measurements have been upscaled to 400 m resolution by averaging and randomly varying noise is added to the upscaled soil moisture values. This provides a simple way to simulate soil moisture retrievals using passive remote sensing. PALS data are used to demonstrate the sensitivity of AIRSAR L-band copolarized channels to soil moisture only.

4.1.3. Data from SMEX02. The algorithm discussed above was tested on data obtained from the Soil Moisture Experiments in 2002 (SMEX02). The SMEX02 campaign was conducted in Walnut Creek, a small watershed in Iowa, over a one-month period between mid-June and mid-July 2002. An extensive dataset of in situ measurements of soil moisture (0–6 cm soil layer), soil temperature (surface, 5 cm depth) soil bulk density, and vegetation water content was collected. Aircraft-mounted instruments—the passive and active, L- and S-band sensor (PALS) and the NASA/JPL airborne synthetic aperture radar (AIRSAR)—were flown with supporting ground-sampling data. The PALS instrument was flown over the SMEX02 region on June 25, 27 and July 1st, 2nd, 5, 6, 7, and 8, 2002 [84, 85]. PALS radiometer and radar provided simultaneous observations of horizontally and vertically polarized L- and S-bands brightness temperatures, radar backscatter measured in VV, HH and VH configurations, and thermal infrared surface temperature at a resolution of ~400 m. The AIRSAR instrument has P-, L-, and C-bands with H/V dual microstrip polarizations and spatial resolutions of 5 m in slant range and 1 m in azimuth [86]. AIRSAR instrument was flown on July 1st, 5, 7, 8, and 9. The algorithm proposed in this study needs simultaneous observations of the radar and radiometer. As the PALS spatial coverage of the watershed on July 1st was partial, the data sets for PALS and AIRSAR for July 5, July 7, and July 8 were used. AIRSAR data used in this study was L band HH and VV polarization and provided at a spatial resolution of 30 m after processing. The AIRSAR images were geolocated by registration to a Landsat TM7 image. The ground-based soil moisture data used in this study was the volumetric soil moisture measured using a theta probe at 14 locations in each field site for all the 31 fields. There were 10 soy fields and 21 corn fields. The representative area for each field site was 800 × 800 m^2. Seven measurements of volumetric soil moisture made along each of two parallel transects, 600 m in length and placed 400 m apart. Higher-resolution estimates of in situ soil moisture for each field were estimated by an inverse-distance-weighted spatial interpolation using all the 14 measurements for each field and a cell size of 100 m.

4.1.4. Results from Radar-Radiometer. As an initial evaluation of radar sensitivity to soil moisture, the AIRSAR L band vertically copolarized backscattering coefficients were aggregated to 800 m and then collocated with the field sites that were sampled for 0–6 cm volumetric soil moisture. Figure 8 presents a plot of the change in 800 m resolution field averages of AIRSAR LVV backscattering coefficient and soil moisture for the periods July 5 to July 7 and July 5 to July 8. The change in soil moisture between July 7 and July 8 was not very high. In order to see a greater change in soil moisture the difference in July 5–July 8 was selected. The R^2 value of 0.57 indicates that $\Delta\sigma^0_{LVV}$ is sensitive to the change in soil moisture; even under the dense vegetation conditions encountered in the SMEX02

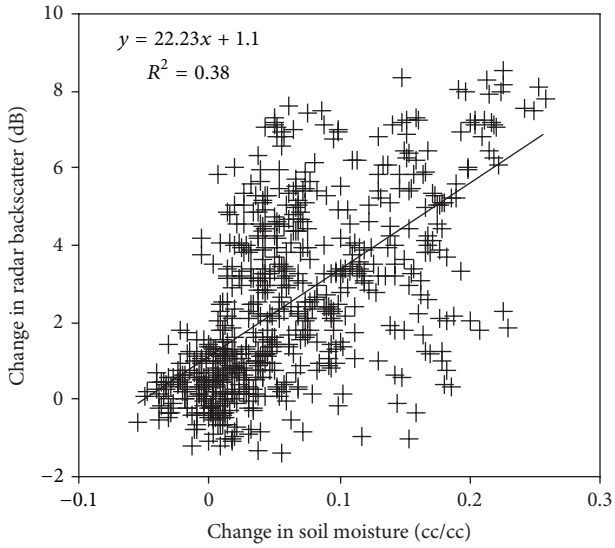

Figure 9: Plot of change in AIRSAR LHH backscatter at 100 m resolution versus change in in situ volumetric soil moisture at 100 m resolution for the periods July 5 to July 7 and July 5 to July 8 [55].

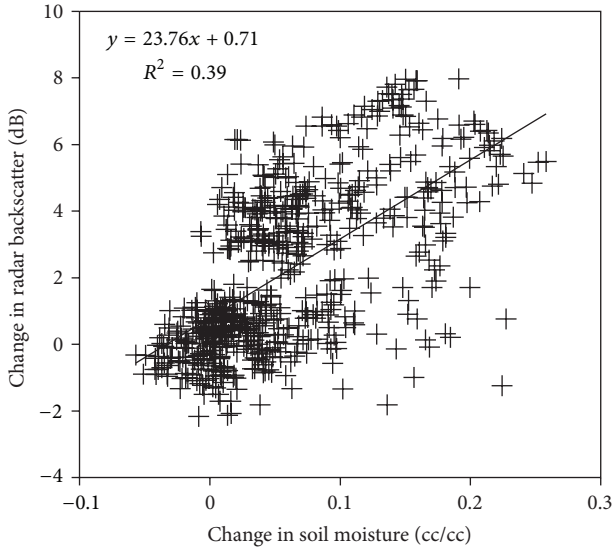

Figure 10: Plot of change in AIRSAR LVV backscatter at 100 m resolution versus change in in situ volumetric soil moisture at 100 m resolution for the periods July 5 to July 7 and July 5 to July 8 [55].

experiments with the vegetation water content of corn fields being around 4-5 kg/m^2.

The sensitivity of the AIRSAR LVV channel to soil moisture was also analyzed at a higher spatial resolution of 100 m. In Figures 9 and 10 the change in radar backscatter (LHH and LVV, resp.) is compared to the corresponding change in gravimetric soil moisture at a resolution of 100 m for the time periods July 5 to July 7 and July 5 to July 8. R^2 values of 0.38 and 0.39 are obtained for LHH and LVV, respectively, indicating that radar sensitivity to soil moisture is significant at the higher spatial resolution of 100 m also. The sensitivities are approximately the same for both LHH and LVV channels with values of 22.2 and 23.8 dB/(cc/cc), respectively. It should be noted that there are several data points in Figures 8, 9, and 10 with negative backscatter change corresponding to positive change in soil moisture. At the 800 m spatial resolution (Figure 8) we see data points with a negative change in the range 0 to −1 dB for change in moisture in the range 0 to 0.05 cc/cc. At the 100 m spatial resolution (Figures 9 and 10) several data points undergo a negative change in the range 0 to −2 dB for change in moisture in the range 0 to 0.1 cc/cc. The authors believe that this effect is primarily due to change in vegetation water content. For example, in Figure 8, pixels increased in moisture from July 5 and July 7 by a small amount (<0.05) but still underwent a negative change in backscatter as the vegetation water content increased from July 5 to July 7 causing a greater attenuation of radar backscatter on July 7 as compared to July 5 to resulting in a negative net change in radar backscatter even though the moisture increased. Soil roughness may also change after a rainfall event causing the soil surface to reduce in roughness and result in lower radar backscatter values after the rainfall event. The assumption made by the author that vegetation and soil roughness do not change between consecutive observations is weak but it also simplifies the problem significantly with satisfactory results in terms of estimated soil moisture change.

It was shown in a previous study that for the SMEX02 field experiment PALS LV channel brightness temperatures were well correlated to soil moisture [41]. A further demonstration of the AIRSAR LVV channel sensitivity to change in soil moisture is done by comparison of the change in PALS LV channel brightness temperatures to the change in AIRSAR LVV channel backscattering coefficients. Figure 11 presents the difference images produced by the change in AIRSAR LVV backscattering coefficients from July 5 to July 7 compared to the change in PALS LV channel brightness temperature for the same period. The spatial patterns corresponding to wet and dry regions in the watershed are very similar for both the PALS and AIRSAR difference images. Regions that became wetter from July 5 to July 7 underwent a reduction in brightness temperature and an increase in backscattering coefficient. (The scales for the two images in Figure 11 are hence inverted to represent the positive change in radar backscatter and negative change in brightness temperature with an increase in soil moisture.) The correlation between PALS LV channel brightness temperature change and AIRSAR LVV channel radar backscatter change is further brought out in Figure 12. Change in AIRSAR backscattering coefficients (LVV) have been aggregated to 400 m resolution and compared with the change in PALS brightness temperatures (LV) at its resolution of 400 m. An excellent agreement is seen between the two with an R^2 value of 0.81 indicating that AIRSAR LVV channel has a significant sensitivity to soil moisture.

The algorithm discussed in the previous section was applied to the 3 days of AIRSAR LVV, PALS LV, and ground-based soil moisture data. 400 m resolution estimates of soil moisture ($m_{v,\mathbf{X}}$) were calculated using the in situ measurements of soil moisture within each field. As mentioned earlier, 14 theta probe measurements of soil moisture were made at

each watershed-sampling site that had dimensions of 800 m by 800 m. The in situ measurements were gridded to a 100 m dimension grid using inverse distance interpolation and then they were upscaled to 400 m corresponding to the dimensions of the PALS radiometer footprint. A uniformly distributed random noise of 0–0.016 g/cc was added to the upscaled in situ soil moisture values in order to simulate 4% maximum error that would be obtained if the soil moisture estimates were obtained by inverting soil moisture estimates from L-band brightness temperatures using a radiative transfer model. AIRSAR LVV data was also aggregated to a resolution of 100 m and the difference images were used to compute $\Delta\sigma^0_x$ where "x" denotes the lower cell size of 100 m. Using the algorithm discussed in the previous section, 100 m resolution estimates of the change in soil moisture were obtained for two periods of July 5 to July 7 and July 7 to July 8 for each field site. Figures 13(a) and 13(b) compare estimated change in soil moisture with measured change in soil moisture at a 100 m resolution for the period July 5 to July 7 and Figures 14(a) and 14(b) present the same comparison for the period July 5 to July 8. The root mean square error for the prediction (RMSE) in both cases is 0.046 cc/cc volumetric, a major portion of which seems to be contributed by a few outliers. It was noted that on removing 7 outliers from the plot in Figure 13(a) and 32 outliers from the plot in Figure 14(a), the RMSE improves to 0.032 cc/cc and 0.024 cc/cc, respectively. The outliers seen in Figures 13 and 14 are caused by the invalidity of the assumption that vegetation and surface roughness do not change significantly during consecutive time steps for few data points. For example, the encircled data point in Figure 13(a) is observed on field WC11 where the observed change in radar backscatter (LVV) was −1.871 dB and with no change in the corresponding change in in situ soil moisture. Table 11 presents the observed change in soil moisture and corresponding change in LVV radar backscatter from July 5 to July 7 for the field WC11. It is seen that although change in soil moisture was low for all data points, the change in corresponding radar backscatter was not low for all pixels. This may be a result of several factors such as significant localized change in vegetation or surface roughness, heterogeneity within the 100 m pixel, such as present of ponded water within the pixel but not at the soil moisture sampling location, human errors in sampling of soil moisture, and errors in geolocation of the AIRSAR data. Such pixels are not numerous and hence were not analyzed in complete detail in the present study. Computation of radar sensitivity when the soil moisture change is low is numerically unstable as $\Delta m_{v,\mathbf{X}}$ appears in the denominator equation (15). It may be possible to develop an alternate approach for computing sensitivity where a time series of radar backscatter and soil moisture observations is used to compute sensitivity using the lowest and highest soil moisture values observed during a period of say 7–10 days during which the change in vegetation and surface roughness can be assumed to be insignificant. Having a greater range of soil moisture values will lead to a more accurate computation of radar sensitivity to soil moisture. The suggested approach has not been attempted in the current study; only 3 days of data were available.

4.2. Downscaling Using Visible and Near Infrared Satellite

4.2.1. Background. In this approach we used the relationship between soil moisture and surface temperature modulated by vegetation. This approach has a background with past studies of Mallick et al. [87] who used the triangular relationship [68, 88–90] between surface temperature and the vegetation index (TvX) derived from the MODIS Aqua sensor data. From this they derived the soil wetness index that was converted to soil moisture at a 1 km scale. Minacapilli et al. [91] used thermal infrared observations from an airborne platform to estimate soil moisture using the thermal inertia principle for a bare soil field. They found that the estimated soil moisture correlated very well with in situ observations. Gillies and Carlson [67] devised a method that derived the fractional vegetation and spatial patterns of soil moisture using the AVHRR data set and demonstrated this method in a region of England. In our method, the diurnal temperature range (DTR) was used [92], which was affected by vegetation [93], soil moisture, and clouds [94].

This section is organized as follows: Section 4.2.2 provides the list of datasets and the locations of our study; Section 4.2.3 outlines the downscaling algorithm methodology. In Section 4.2.4 we discuss our findings and validation of the results. The results and discussion are presented in Section 4.2.4.

4.2.2. Data. Oklahoma was selected as the study area due to the long history of soil moisture research focused on this region. The Oklahoma Mesonet and Little Washita River Experimental Watershed are two long-term in situ soil moisture networks which provide a solid foundation for soil moisture remote sensing research (shown in Figure 15). The Little Washita has been the location for various soil moisture field experiments including SGP97, SGP99, and SMEX03 [95, 96] and has been a key element in satellite validation studies [97, 98]. In addition to the ground resources, a variety of spaceborne sensors also contributed to this study. Descriptions and maps of the datasets used in this article are shown in Table 12 and Figure 16. Table 12 lists the spatial resolution and temporal repeat of these sensors and their data products.

(1) *NLDAS Data.* The NLDAS (North American Land Data Assimilation System, http://ldas.gsfc.nasa.gov/nldas/) phase 2 hourly mosaic data is used in this study. NLDAS is run hourly on a geographical grid with a spatial resolution of 1/8° (12.5 km). The NLDAS-2 data output includes various surface variables, such as radiation flux, surface runoff, surface temperature, vegetation indices, and soil moisture [99]. Soil, vegetation, and elevation are parameterized using high-resolution datasets (1 km satellite data in the case of vegetation). The forcing data [100, 101] and outputs have been extensively validated [102–104]. The soil moisture downscaling model in this study utilized two variables: surface skin temperature and soil moisture content at 0–10 cm depths. The data used in this study correspond to the closest local

overpass times of Aqua satellite for the Oklahoma region, which are approximately 8:00 and 20:00 PM (in UTC time).

(2) *AMSR-E Data.* The Advanced Scanning Microwave Radiometer on board the EOS Aqua platform (AMSR-E) collected microwave observations at 6, 10, 19, 37, and 85 GHz from 2002 to 2011 [105]. The AMSR-E instrument provided global passive microwave measurements of terrestrial, oceanic, and atmospheric parameters for hydrological studies from 2002–2011 [105, 106]. The soil moisture product derived from the AMSR-E sensor on board the Aqua satellite has 1/4° (25 km) spatial resolution. The estimation of AMSR-E soil moisture accuracy is approximately 10% and cannot be estimated in the area of vegetation biomass which is greater than 1.5 kg/m^2 [73].

In this study, the AMSR-E soil moisture was estimated by using the single-channel algorithm (SCA) [97, 107]. The single-channel algorithm uses the X-band observations at h-polarization (the most sensitive channel). The C-band observations cannot be used for land surface applications because they are significantly affected by manmade radio frequency interference (RFI). The land surface temperature was estimated using the 37 GHz v-pol observations. AVHRR-derived climatological dataset was used to correct for vegetation effects. For matching with other georeferenced datasets, a drop-in-the-bucket method was applied to the AMSR-E data and it was gridded to a 25 × 25 km EASE grid cell size. This method averaged all the AMSR-E points by determining if their center coordinates were within the borders of a particular EASE grid cell.

(3) *MODIS Data.* The surface temperature data which corresponded to the local time of 1:30 and 13:30, as well as the NDVI from MODIS/Aqua, were used in this study. MODIS has 36 spectral bands including visible, near infrared, and thermal infrared spectrum and provides 44 global data products [108]. The algorithms to derive the MODIS products are well established and have been extensively evaluated, including NDVI [109, 110], LAI [111], land cover classification [62, 112], and surface temperature [113]. In the current study surface temperature and NDVI products at two different spatial resolutions were used for downscaling soil moisture. The datasets included 1 km daily surface temperature (MYD11A1), 1 km biweekly NDVI (MYD13A2), and 5600 m biweekly Climate Modeling Grid (CMG) NDVI (MYD13C1). In addition, the dry down curves of soil moisture during May 2004, July 2005, and August 2005 in Oklahoma were examined. During these three months, clear days (due to the requirement of surface temperature in our algorithm) of 1 km surface temperature along with low cloud cover were selected for the downscaling algorithm application.

(4) *AVHRR Data.* For the years 1981–2001, prior to the launch of the Aqua satellite and the availability of MODIS data, the 5 km CMG daily NDVI data from AVHRR sensor (AVH13C1) was used. The AVHRR sensor is on board the NOAA satellites, including N07, N09, N11, and N14, and provides global and long-term surface ground measurements. Daily AVHRR NDVI data is available between 1981–1999 (http://ltdr.nascom.nasa.gov/ltdr/ltdr.html). After 2000, the N14 orbit drifted greatly, which can degrade the data quality. Therefore, the years between 2000–2002 were not used in this soil moisture downscaling exercise.

Table 11: Change in in-situ soil moisture (cc/cc) and corresponding change in radar backscatter (LVV) from July 5th to July 7th for the field WC11 at a 100 m spatial resolution [55].

Field	$\Delta\theta$	$\Delta\sigma$
WC11	−0.009	1.431
WC11	−0.007	0.356
WC11	−0.039	−0.049
WC11	0.000	−1.871
WC11	−0.004	−1.081
WC11	−0.005	−0.546
WC11	−0.034	−0.842
WC11	−0.011	−0.816
WC11	−0.013	0.028
WC11	−0.001	−1.419

(5) *Oklahoma Mesonet Data.* The Oklahoma Mesonet is a network of 120 automated environmental monitoring stations with at least one site in each of the 77 counties of Oklahoma [114]. The environmental variables are obtained at intervals spanning every 5 to 30 minutes depending on the variable. The data quality is verified by a series of automated and manual checks via the Oklahoma Climatological Survey [45]. In this investigation, 5 cm soil water content measurement from 116 stations was extracted and geolocated for comparison with the 1 km downscaled, AMSR-E, and NLDAS soil moisture values. The locations of the Oklahoma Mesonet stations are denoted by open yellow circles in Figure 15.

(6) *Little Washita Watershed Data.* The Little Washita Watershed is located in the southwestern portion of Oklahoma and 20 stations are located within a 25 km by 25 km region referred to as the Little Washita Micronet. The watershed soil moisture estimates from the most reliable stations with the closest time to the Aqua overpass time were extracted and then averaged for validation [84, 97]. The locations of these stations are denoted by red dots in Figure 15.

4.2.3. Methodology

(1) *Daily NDVI Interpolation.* Because the MODIS sensor is influenced by cloud cover, only biweekly MODIS radiances were used to calculate the NDVI products at different spatial resolutions. The daily NDVI varies in a near-sinusoidal fashion through all the days every year. To provide NDVI estimates on a daily basis, 13 daily NDVI values of each year (except 2002) and the NDVI obtaining day of the years between 2003–2011 were fitted by using the sinusoidal method as

$$\mathrm{NDVI}_d = a_0 \sin\left(a_1 * D + a_2\right) + a_3, \tag{19}$$

where a_0, a_1, a_2, and a_3 are the regression coefficients, NDVI_d is the daily NDVI value, and D is the day of the year.

Table 12: Sources of land surface data used in the downscaling of soil moisture and their spatial resolution and temporal repeat [61].

Source	Data	Spatial resolution	Temporal repeat
NLDAS	Soil moisture content (0–10 cm layer, kg/m^2)	1/8 degree (12.5 km)	Hourly
	Surface skin temperature (K)	1/8 degree (12.5 km)	Hourly
AVHRR	Normalized difference vegetation index (NDVI)	5 km	Daily
MODIS	Normalized difference vegetation index (NDVI)	5 km	Biweekly
	Land surface temperature (K)	1 km	Daily
AMSR-E	Soil moisture content (m^3/m^3)	1/4 degree (25 km)	Daily
Mesonet	Surface soil water content (0–5 cm layer)	116~117 stations	5 minutes
Little Washita Watershed	Soil moisture measurement (0–5 cm layer)	9 stations	Hourly

This equation was applied to the 5 km NDVI data for all years to obtain daily 5 km NDVI values. Then, the interpolated results were resampled to 12.5 km to match up with NLDAS pixels. Similarly, the daily 1 km NDVI maps for the three months studied in this paper were generated using this method.

(2) *Thermal Inertia Theory.* The concept of thermal inertia is, namely, the resistance of a material to temperature change, which is indicated by the time-dependent variations in temperature during a full heating/cooling cycle. It is defined as the square root of the product of the material's bulk thermal conductivity and volumetric heat capacity, where the latter is the product of density and specific heat capacity:

$$I = \sqrt{k\rho c}, \tag{20}$$

where k is the coefficient of thermal conductivity, ρ is density, and c is the specific heat capacity.

An approximation to thermal inertia can be obtained from the amplitude of the diurnal temperature curve. The temperature of a material with low thermal inertia will change significantly during the day, while the temperature of a material with high thermal inertia will not change as much. The volumetric heat capacity depends on soil moisture. There have been many such attempts in the past since HCMM (Heat Capacity Mapping Mission), the first of a series of Applications Explorer Missions (AEM) [115]. The objective of the HCMM was to provide comprehensive, accurate, high-spatial-resolution thermal surveys of the surface of the earth to determine thermal inertia.

Therefore, it is our assertion that lower values of daily average soil moisture θ^{av} will correspond to higher value of daily temperature difference ΔT_s and vice versa. ΔT_s can be described as

$$\Delta T_s = T_{\max} - T_{\min}, \tag{21}$$

where $T_{\max}$, $T_{\min}$ are the daily highest and lowest temperatures, respectively. The two local overpass times of MODIS approximately correspond to the highest and lowest temperatures.

(3) *Construction of the Downscaling Model.* The MODIS sensor provides two very important products: NDVI and surface temperature (T_s). In this study, these two variables were extracted for each 1 km MODIS pixel (i, j) in the 1/4° gridded AMSR-E radiometer data. We denote these variables by NDVI (i, j) and $T_s(i, j)$. The radiometer-derived soil moisture θ corresponds to the daytime 13:30 overpass θ^a and nighttime 1:30 overpass θ^p for the entire 1/4° pixel. The daytime and the nighttime overpass soil moisture values for each of the MODIS pixels are referred as $\theta^a(i, j)$ and $\theta^p(i, j)$. The average value of the pixel soil moisture is denoted by $\theta^{\text{av}}(i, j)$ which refers to the arithmetic mean of the soil moisture for the 1 km pixel for the morning and night overpass. These are depicted in Figure 17. The MODIS sensor on Aqua was used because it matched the time of AMSR-E soil moisture estimates.

There are three theories that motivate the pixel-based downscaling algorithm. First, we must consider that the soil moisture history of each pixel is unique with regard to precipitation, surface overflow, and runoff and can be summarized by the average soil moisture $\theta^{\text{av}}(i, j)$. Also, based on the thermal inertia theory, the thermal inertia and soil moisture depend on soil thermal conductivity, which for a wet pixel will show a smaller change while a dry pixel will show larger change in surface temperature [91]. Finally, vegetation biomass of each pixel will vary and can modulate the change of surface temperature, which is represented by the daily temperature difference ΔT_s [49, 116]. The comparison of the pixel sizes between the three datasets and the look-up curve building method is shown in Figure 17.

The key to the proposed disaggregation procedure is establishing the relationship between the change in surface temperature and the average soil moisture for the 1 km pixel.

Since the NLDAS-2 data are at 1/8° resolution while the AMSR-E data are at 1/4° resolution, 4 NLDAS-2 pixels are within each AMSR pixel. To construct the look-up curves, we used the NLDAS-2 output plotted separately for each month (12 plots for each 1/4° pixel). For each plot, we used data from all the months of the study period (i.e., the July plot will have data for the surface temperature change and the average soil moisture for all years from 1979 to present). The data for equal NDVI lines at increments of 0.3 in NDVI was subsequently organized. For example, during some months (e.g., January), the vegetation growth was limited and few NDVI curves in the Upper Midwest were constructed (maybe one corresponding to NDVI of 0 and another corresponding to NDVI of 0.3). On the other hand, during other periods,

Table 13: Comparison statistics between the 1 km downscaled, NLDAS, and AMSR-E soil moisture compared to the Oklahoma Mesonet for 6 relatively clear days. RMSE, bias, and standard deviations are in (m^3/m^3) [61].

Day	Dataset	R^2	RMSE	Standard deviation	Bias
May 9, 2004	1 km downscaled	0.223	0.119	0.043	−0.112
	AMSR-E	0.050	0.129	0.053	−0.114
	NLDAS	0.171	0.105	0.074	−0.077
May 22, 2004	1 km downscaled	0.360	0.128	0.044	−0.123
	AMSR-E	0.161	0.114	0.059	−0.100
	NLDAS	0.264	0.108	0.077	−0.084
July 17, 2005	1 km downscaled	0.020	0.168	0.055	−0.155
	AMSR-E	*	0.160	0.063	−0.136
	NLDAS	0.005	0.099	0.059	−0.068
July 21, 2005	1 km downscaled	0.031	0.130	0.047	−0.115
	AMSR-E	0.001	0.143	0.053	−0.126
	NLDAS	0.002	0.106	0.056	−0.081
August 9, 2005	1 km downscaled	0.010	0.167	0.050	−0.155
	AMSR-E	0.005	0.146	0.050	−0.130
	NLDAS	0.006	0.103	0.055	−0.074
August 18, 2005	1 km downscaled	0.225	0.166	0.058	−0.158
	AMSR-E	0.387	0.160	0.053	−0.154
	NLDAS	0.114	0.106	0.064	−0.075

* <0.001.

Table 14: Comparison statistics between the 1 km downscaled, NLDAS, and AMSR-E soil moisture compared to the Little Washita soil moisture observations for 6 relatively clear days. RMSE, bias, and standard deviations are in (m^3/m^3) [61].

Day	Dataset	Number of points	RMSE	Standard deviation	Bias
May 4, 2004	1 km downscaled	8	0.043	0.015	0.009
	AMSR-E	3	—	—	−0.019
	NLDAS	6	0.040	0.020	0.016
May 6, 2004	1 km downscaled	8	0.077	0.015	0.032
	AMSR-E	3	—	—	0.005
	NLDAS	6	0.055	0.017	0.035
July 3, 2005	1 km downscaled	6	0.066	0.070	0.006
	AMSR-E	3	—	—	0.010
	NLDAS	4	0.061	0.070	0.020
July 17, 2005	1 km downscaled	2	0.050	0.015	0.047
	AMSR-E	2	—	—	0.031
	NLDAS	2	0.057	0.015	0.056
August 2, 2005	1 km downscaled	7	0.031	0.019	0.024
	AMSR-E	3	—	—	0.027
	NLDAS	4	0.048	0.014	0.046
August 4, 2005	1 km downscaled	7	0.022	*	0.022
	AMSR-E	3	—	—	0.023
	NLDAS	4	0.048	0.010	0.047

* <0.001.

such as July in the Upper Midwest, rapid changes in NDVI due to crop growth could occur and many NDVI curves ranging from NDVI of 1.0 to 5.0 would be created. The curves were fitted to these points—930 points corresponding to the AMSR-E am overpass time (30 years of July data × 31 days) and 930 points corresponding to AMSR-E pm overpass time.

A simple linear regression model between the daily average soil moisture $\theta^{\text{av}}(i, j)$ and daily temperature difference $\Delta T_s(i, j)$ for all 30 years for each month was developed as follows:

$$\theta^{\text{av}}(i, j) = a_0 + a_1 \Delta T_s(i, j), \quad (22)$$

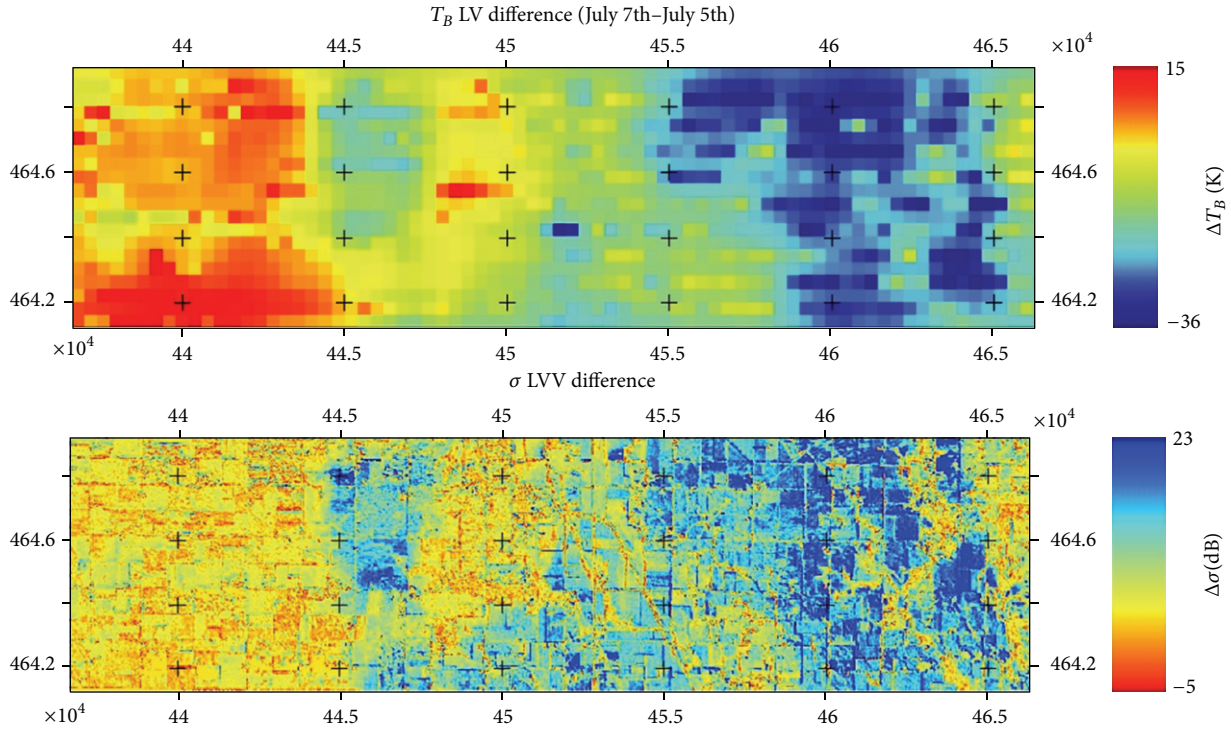

Figure 11: Difference images for change in PALS LV brightness temperatures at 400 m resolution and change in AIRSAR LVV backscatter at 30 m resolution for the period July 5 to July 7 (July 5–July 7). The spatial patterns corresponding to wetting or drying are strikingly consistent in both images indicating that the AIRSAR LVV channel is sensitive to near-surface soil moisture [55].

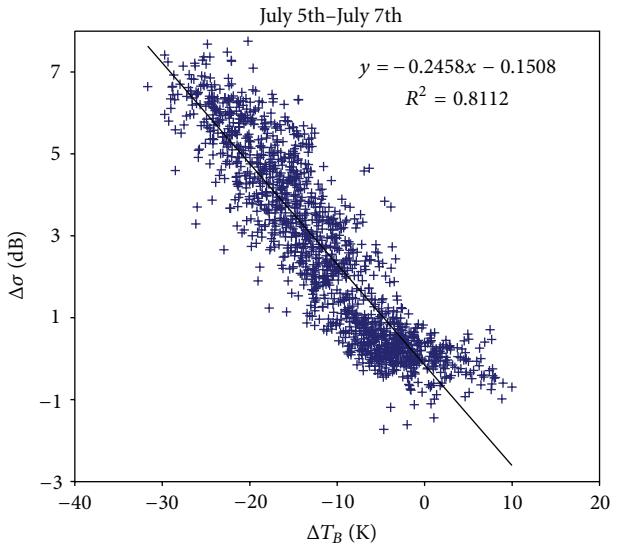

Figure 12: Chance in PALS L band V pol. brightness temperature plotted versus change in AIRSAR LVV channel backscattering coefficients. AIRSAR data has been aggregated to the PALS resolution of 400 m. Change is computed for the days July 5 to July 7 [55].

where i, j represent the pixel location. a_0 and a_1 are regression model coefficients which correspond to several different NDVI intervals. The growing season between May–September was examined in this study and the NDVI was subdivided to three intervals: 0~0.3, 0.3~0.6, and 0.6~1. For each month, three NLDAS-based look-up curves of each pixel, which corresponded to the three NDVI intervals were built and the regression coefficients, were obtained.

(4) *Correction of 1 km Downscaled Soil Moisture.* On a daily basis, we used the curves corresponding to the NLDAS-2 data closest to the MODIS pixel to calculate the 1 km $\theta^{\mathrm{av}}(i, j)$ from the $\Delta T_s(i, j)$ of each 1 km MODIS pixel. We then averaged $\theta^{\mathrm{av}}(i, j)$ from all the 1 km MODIS pixels and compared the values to daily average AMSR-E soil moisture $(\Theta^a + \Theta^p)/2$ and then corrected each $\theta^{\mathrm{av}}(i, j)$ with the difference between $(\Theta^a + \Theta^p)/2$ and $\theta^{\mathrm{av}}(i, j)$. The corrected soil moisture $\theta^{\mathrm{avc}}(i, j)$ is given by

$$\theta^{\mathrm{avc}}(i, j) = \theta^{\mathrm{av}}(i, j) + \left[\left(\frac{\Theta^a + \Theta^p}{2}\right) - \frac{1}{N}\sum_{i,j}\theta^{\mathrm{av}}(i, j)\right]. \tag{23}$$

We subsequently generated daily values of $\theta^{\mathrm{avc}}(i, j)$ at 1 km. This satisfies the following conditions: (a) the average of the disaggregated soil moistures over the AMSR-E pixel is the same as that recorded by AMSR-E, (b) the MODIS 1 km vegetation modulates the distribution of the disaggregated soil moisture through its influence in the change in surface temperature to morning and evening averaged soil moisture computed by NLDAS, and (c) the 1 km scale changes in surface temperature reflect on soil moisture distribution as evidenced in the disaggregated soil moisture. In addition, this

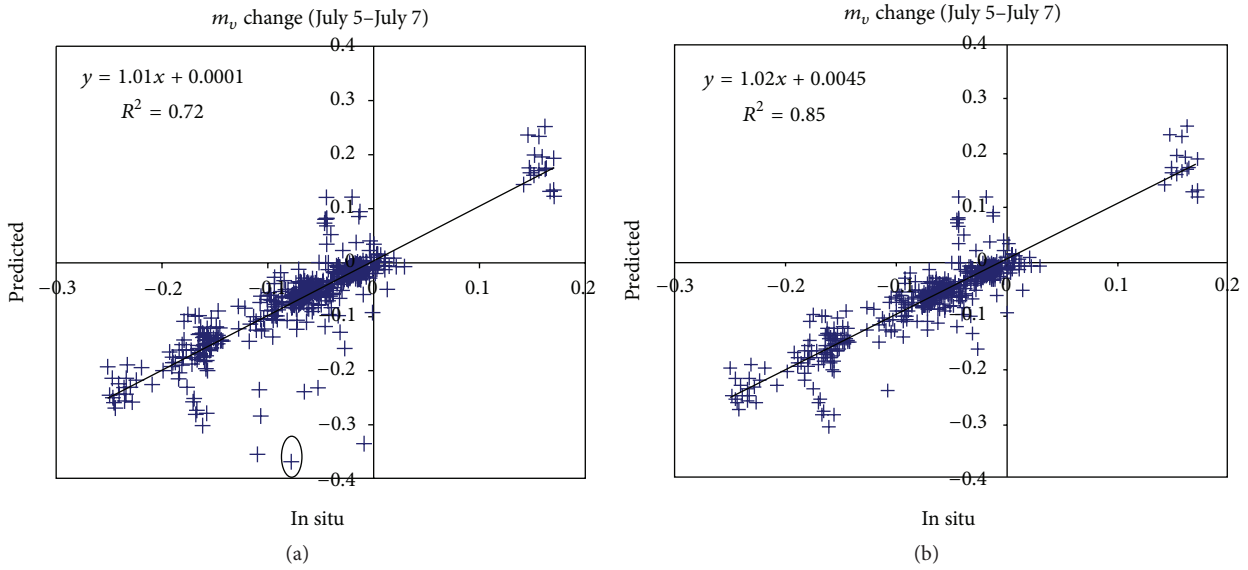

Figure 13: 100 m in situ soil moisture change (x-axis) compared with the 100 m resolution estimates of soil moisture change derived from the algorithm for the period July 5 to July 7. Plot (a) has all the points with RMSE = 0.046, and plot (b) has 7 outliers removed with RMSE = 0.032 [55].

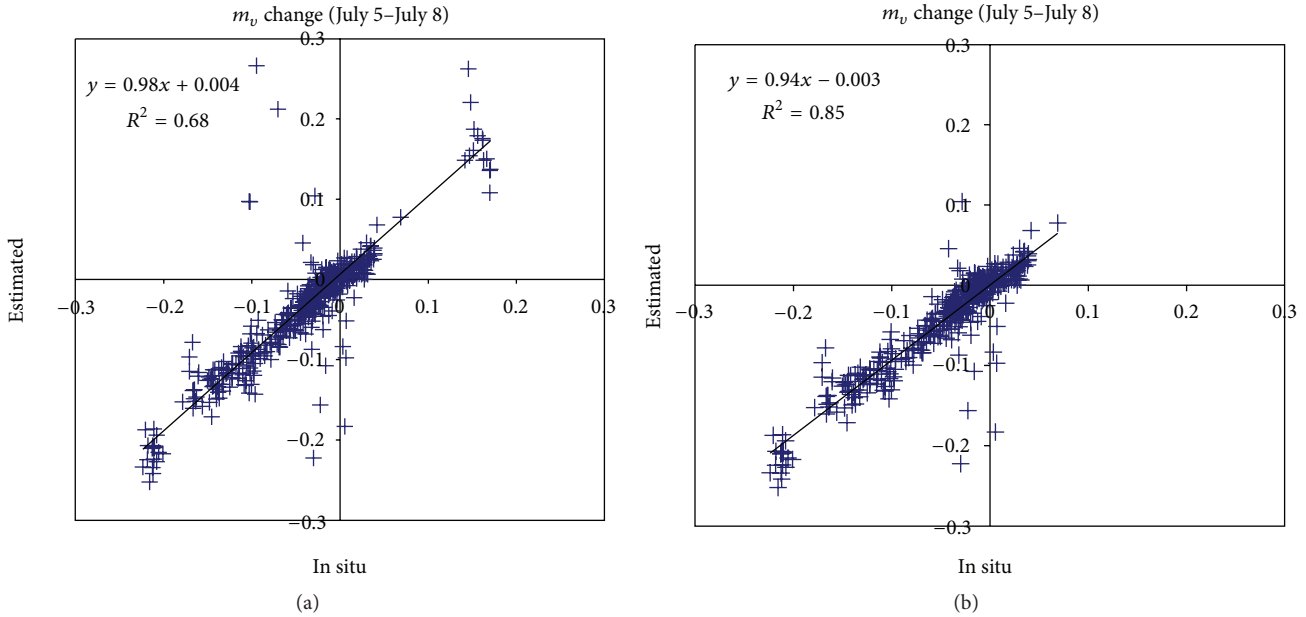

Figure 14: 100 m in situ soil moisture change (x-axis) compared with the 100 m resolution estimates of soil moisture change derived from the algorithm for the period July 5 to July 8. Plot (a) has all the points with RMSE = 0.046, and plot (b) has the data points from fields WC30 and WC31 removed resulting in an RMSE of 0.024 [55].

methodology can only be applied over areas with no cloud cover.

4.2.4. Results

(1) $\theta^{av} - \Delta T_s$ *Look-Up Curves.* Figure 18 shows the regression fitting results between NLDAS-derived daily temperature difference and daily average soil moisture of a pixel (latitude: 101.875°W~102°W; longitude: 35.125°N~35.625°N) for the three growing months: May, July, and August. It can be noticed that the daily average soil moisture values for all the months are in the range from 0.05~0.3. The points that correspond to each NDVI interval (0–0.3, 0.3–0.6, and 0.6–1.0) yield nearly parallel lines and the R^2 value of the fit for July are 0.54, 0.56, and 0.40, respectively, for each NDVI

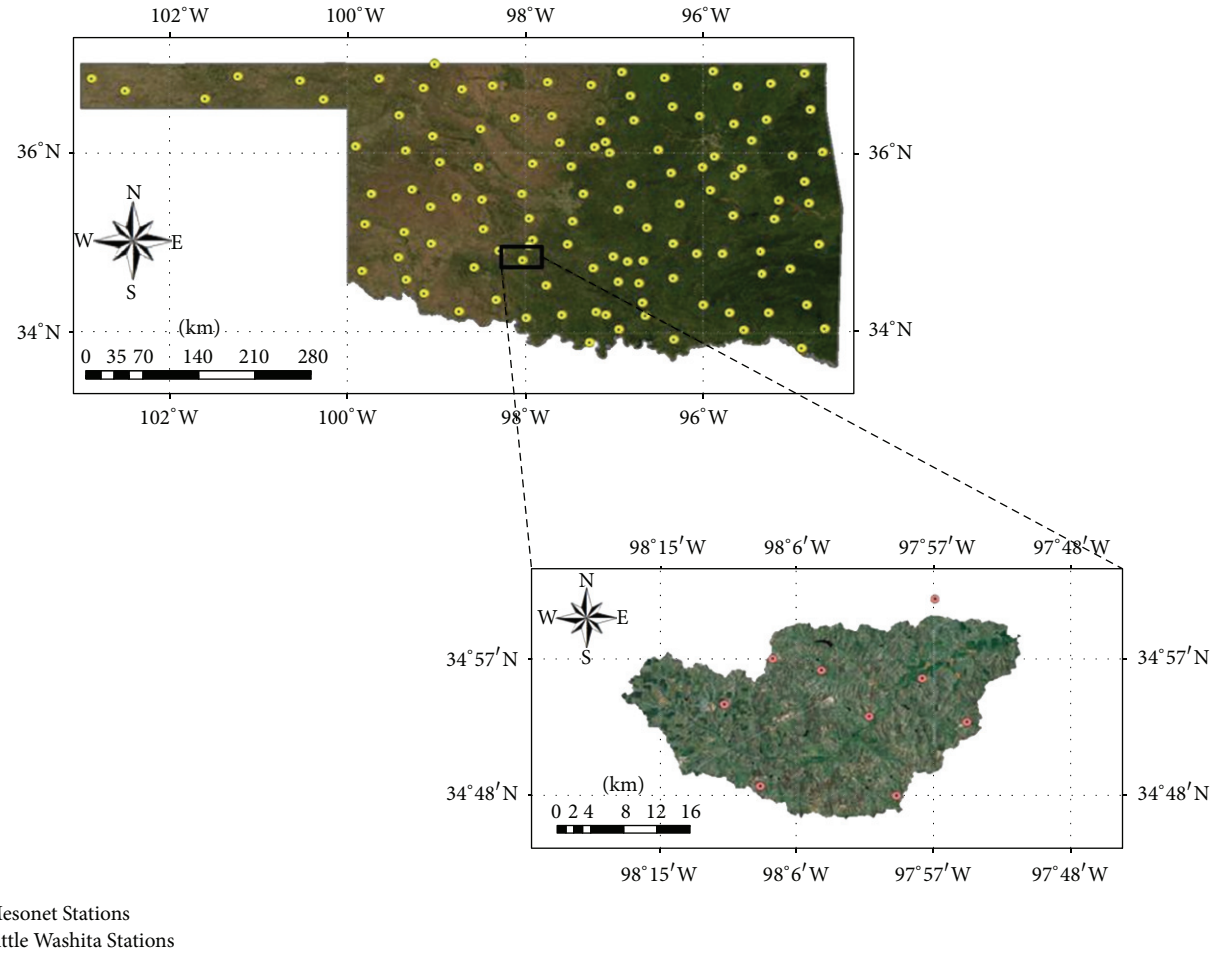

Figure 15: Imagery maps of study region of Oklahoma and the Little Washita Watershed. The locations of the Mesonet Stations are denoted in open yellow circles and the soil moisture sites for Little Washita are noted in red dots [61].

interval. Further, the daily average soil moisture has a negative relationship with the daily temperature change which is consistent with the assumptions that (a) the temperature change between morning and night is determined by the wetness of pixel and (b) the vegetation modulates the change of surface temperature and the pixel with higher vegetation is less sensitive to the temperature change.

(2) *1 km Downscaled Soil Moisture Analysis.* Three maps of daily 1 km downscaled soil moisture are shown as examples: May 22, 2004, July 17, 2005, and August 9, 2005 (Figure 19). The 1 km downscaled soil moistures in the lower Mideast part of Oklahoma are missing, which may be due to two reasons: (a) precipitation and heavy cloud cover often dominate this area especially in growing season which may result in missing MODIS surface temperature data and (b) this area corresponds to a gap between AMSR-E sensor swaths. These downscaled maps illustrate the pattern of soil moisture distribution whereby the soil moisture content gradually increases from west to east, which roughly corresponds to the NDVI variation in Oklahoma. In addition, the 1 km downscaled soil moisture maps also exhibit similar patterns as those of AMSR-E and NLDAS.

For each of the days depicted in Figures 20(a)–20(c), the comparison of the 1 km downscaled soil moisture is shown on the top panel, the AMSR-E 1/4° soil moisture in the central panel, and the NLDAS 1/8° soil moisture in the bottom panel. The NLDAS soil moisture always has complete coverage because it is not impacted by cloud cover or missing data due to swaths not overlapping with each other. On May 22, 2004, a wet area existed in the northeast corner of Oklahoma and this was not captured by the AMSR-E or the 1 km downscaled soil moisture. Even so, in general the spatial patterns of the three estimates resemble each other for the May 22, 2004, case. On July 17, 2005, the western half of Oklahoma was very dry with soil moisture close to 0.02 with larger values in the east. The spatial structure shown by the 1 km soil moisture shows variability even in the dry western part of the state, which cannot be observed using the 1/4° AMSR-E estimates alone. In addition, the 1 km soil moisture captures the wet area in the east central part of the state. A similar west-to-east dry-

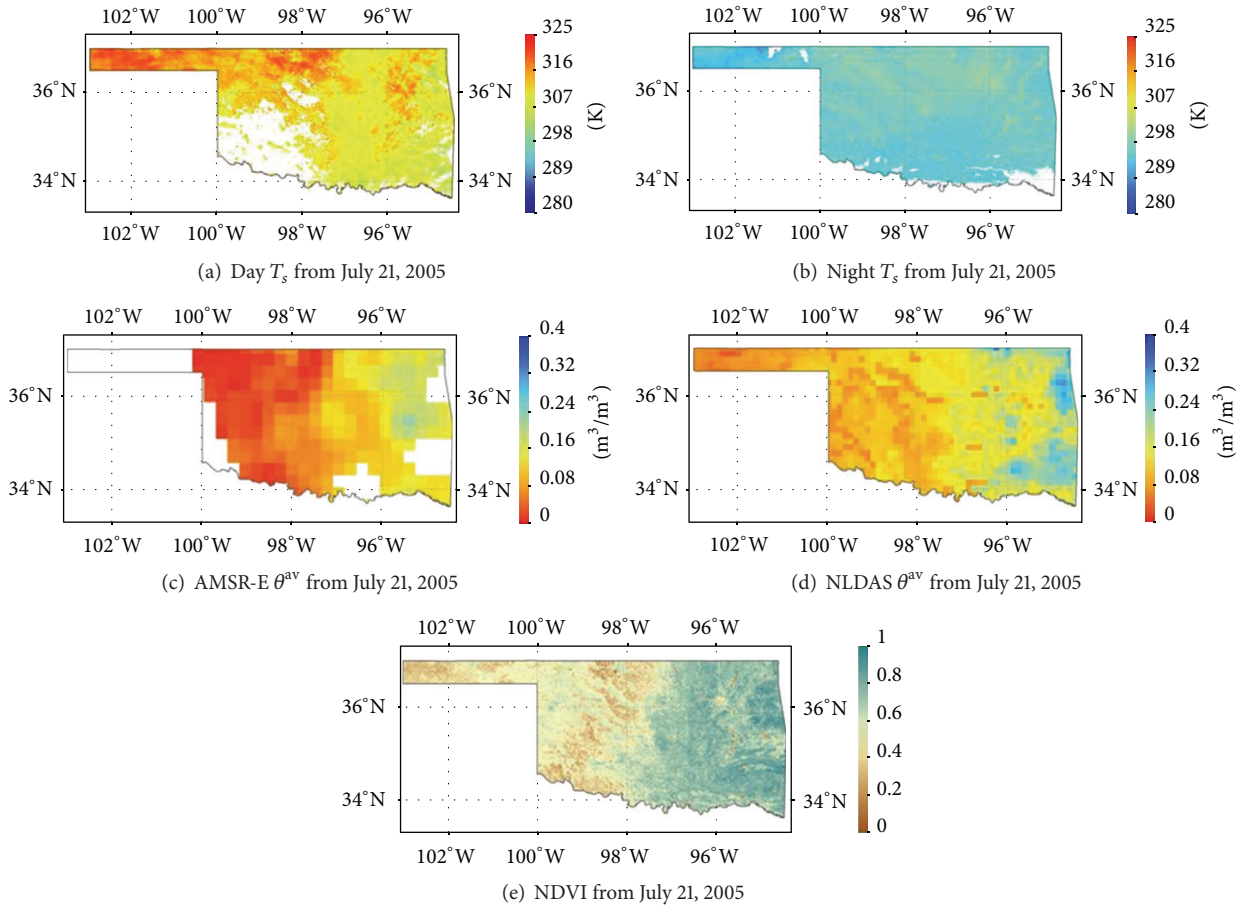

FIGURE 16: Maps of Variables used in the soil moisture downscaling algorithm from July 21, 2005, over Oklahoma (a) MODIS Aqua 1 km land surface temperature during the day. (b) MODIS Aqua 1 km land surface temperature at night. (c) 1/4° spatial resolution AMSR-E soil moisture. (d) 1/8° spatial resolution NLDAS soil moisture. (e) MODIS Aqua 1 km NDVI [61].

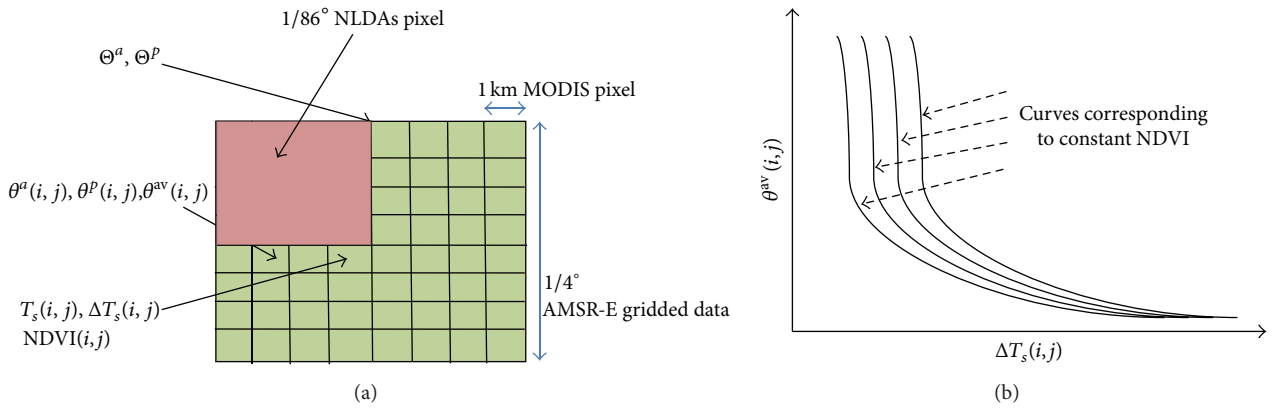

FIGURE 17: (a) Shows the various elements in the disaggregation procedure and (b) shows construction of the curves corresponding to constant NDVI between average soil moisture and change in surface temperature [61].

to-wet pattern was observed in all the estimates of the soil moisture for August 9, 2005.

(3) *Validation by Oklahoma Mesonet Soil Moisture Data.* Table 13 shows that the R^2 values of the 1 km downscaled soil moistures are better than AMSR-E and NLDAS, which range from 0.01~0.36, RMSE (range from 0.119~0.168 m^3/m^3), standard deviation (range from 0.043~0.058 m^3/m^3), and bias (ranges from −0.158~−0.112 m^3/m^3). The R^2 values for NLDAS ranges from 0.002 to 0.264 and those for AMSR-E

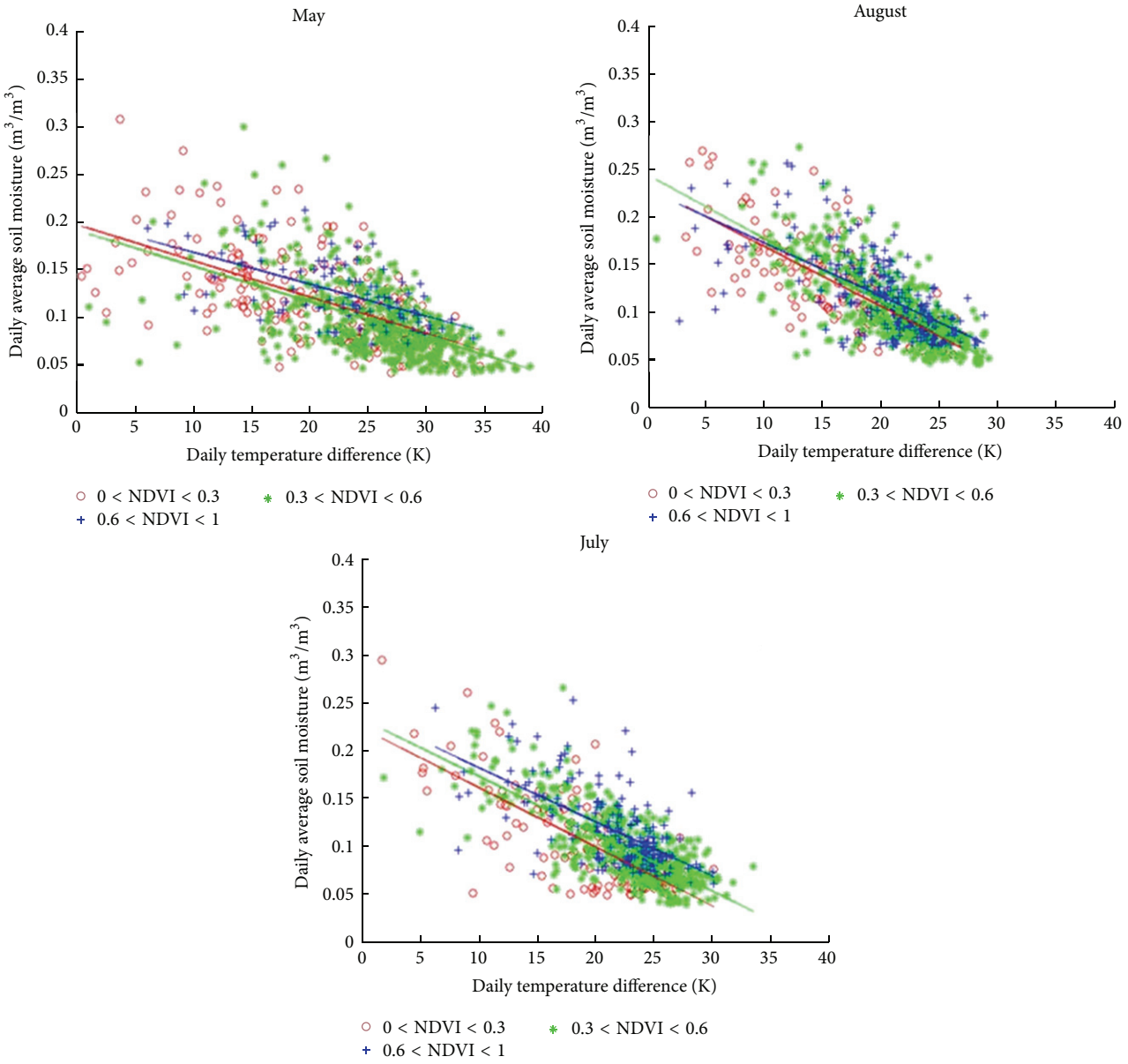

Figure 18: Daily temperature difference versus daily average soil moisture corresponding to latitude: 101.875°W~102°W; longitude: 35.125°N~35.625°N and different NDVI values for May, June, and July [61].

from <0.001 to 0.387. These values are considerably lower than those corresponding to the 1 km downscaled soil moistures. Besides, the RMSE values for NLDAS and AMSR-E range from 0.099~0.108 m^3/m^3 and 0.114~0.160 m^3/m^3, respectively, which are similar to the range of 1 km downscaled soil moistures. Comparing the correlation scatter plots of the three datasets versus the Mesonet data (Figures 20(a)–20(c)), it can be seen that the 1 km downscaled soil moisture has fewer points than AMSR-E and NLDAS. The reason for this is due to cloudiness and the lack of availability of the surface temperature. Thus it was not possible to downscale the AMSR-E soil moisture to produce the 1 km soil moisture.

It should be noted that the soil moisture values of all three datasets are biased, which indicate that the simulated soil moisture values are lower than the in situ Mesonet observation values. This could be attributed to the following. (a) The accuracy of AMSR-E soil moisture is limited and approximately 0.10. This methodology is based on preserving the 25 km mean soil moisture same as the AMSR-E soil moisture estimates. So, any overall day-to-day bias present in the AMSR-E soil moisture retrievals will be present in the disaggregated 1 km estimates. (b) The MODIS-retrieved daytime surface temperature is higher than the NLDAS-2 land surface model output, particularly during the growing season, which may be the cause of the daily temperature difference being greater than NLDAS and consequently the downscaled soil moisture being lower than NLDAS. (c) The Oklahoma Mesonet consists of Campbell Scientific

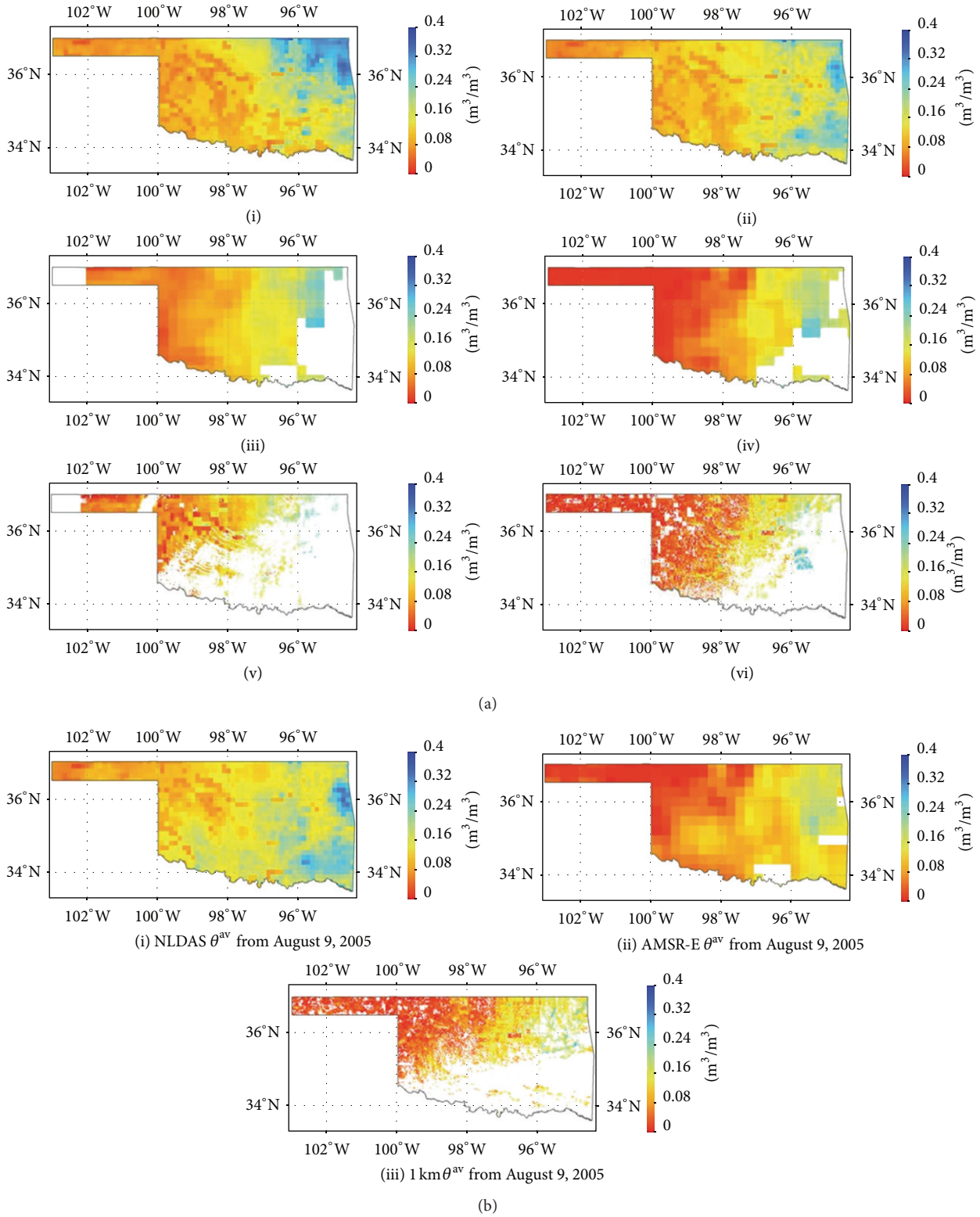

FIGURE 19: (a) Maps of the NLDAS, AMSR-E, and 1 km soil moisture (m^3/m^3) from May 22, 2004 ((i)–(iii)) and July 17, 2005 ((iv)–(vi)); (b) maps of the NLDAS, AMSR-E, and 1 km soil moisture (m^3/m^3) from August 9, 2005 [61].

229-L sensors which are soil matric potential sensors (then converted to volumetric soil moisture) which may have biases when compared to the gravimetric and neutron probe samples, of which RMSE is between 0.006~0.052 [45].

(4) *Validation Using Little Washita Watershed Soil Moisture Data.* Table 14 shows the statistical results for six days of Little Washita Watershed soil moisture comparisons with 1 km downscaled, AMSR-E, and NLDAS. AMSR-E statistics are not shown because these were less than three points of AMSR-E soil moisture over this period. Since the comparisons require high coverage of valid 1 km downscaled soil moisture values within the Little Washita region, the days used for the Little Washita comparisons are different from those used for the Mesonet comparisons. Two clear days from each month, (May 4, 2004, May 6, 2004, July 3, 2005, July 17, 2005, August 2, 2005, and August 4, 2005) were selected. In addition, the correlation plots including four clear days and the total 15 clear days of soil moisture in May in the Little Washita region versus the 1 km, AMSR-E, and NLDAS soil moisture are presented in Figures 21 and 22.

For the 1 km downscaled soil moisture, the RMSE values range from 0.022~0.077, while the standard deviations range from <0.001~0.07 and bias ranges from −0.047~0.032. These statistical results demonstrate that the 1 km downscaled soil moisture values are equivalent to the NLDAS and better than the accuracy of AMSR-E soil moisture values. In addition, the downscaled soil moisture values have a higher spatial resolution than the NLDAS soil moisture values since they are at 1 km as opposed to 12.5 km for NLDAS. This will be particularly important in small watershed studies when one pixel of NLDAS might cover the whole catchment and not provide information on spatial variability. Moreover, the results also indicate that the 1 km downscaled soil moisture has a better agreement with Little Washita than Mesonet, although the variables of July 17, 2005, do not perform as well as the other days.

By analyzing the single days correlation plots for May (Figures 21–22), it can be seen that the 1 km downscaled soil moistures match up well with the AMSR-E and NLDAS soil moistures. The correlation for the May 2004 1 km downscaled results versus the Little Washita soil moisture was $R^2 = 0.4$ with an RMSE of 0.018. The statistical results are also better than the comparison with Mesonet soil moistures. A small catchment such as the Little Washita might be covered by only a single pixel of AMSR-E pixel or a few NLDAS pixels; the downscaled soil moisture offers the distinct advantage of having many more pixels (900 1 km pixels versus 6 NLDAS pixels for Little Washita Watershed) and provides spatial variability information.

The frequency distribution of the differences between Little Washita soil moisture values versus 1 km downscaled, AMSR-E, and NLDAS soil moisture values are presented in Figures 23(a)–23(c), respectively. For the Little Washita soil moisture values within a particular AMSR-E or NLDAS are averaged; their correlation plots have fewer points than the 1 km downscaled soil moisture values. The results indicate that the differences between the 1 km downscaled soil moistures and Little Washita results generally distribute range from −0.05–0.1 and the differences of downscaled soil moisture is around 7%–36% of the total, which is similar to the NLDAS.

5. Conclusions and Discussions

Since this paper has discussed three major studies the conclusions from each of them will be highlighted separately in the subsections below. In Section 5.1 the results from the field experiment study of SMEX02 conducted in Ames, Iowa, in summer 2002 will be discussed. The major findings from the study on disaggregation of passive microwave data using active radar observations will be dealt with in Sections 5.2 and 5.3 will explain the major findings from the use of visible near infrared data in disaggregation of AMSR-E data over Oklahoma.

5.1. Use of PALS in the SMEX02 Field Experiment. This section applied existing algorithms to previously untested conditions of vegetation cover. The sensitivity of PALS radiometer and radar to soil moisture in these conditions has been studied. Soil moisture retrievals were performed using statistical as well as physical modeling techniques. The root mean square error associated with soil moisture retrieval by statistical regression was around 0.051 g/g while soil moisture retrieval using the zero order incoherent radiative transfer model gave retrieval errors of around 0.036 g/g gravimetric soil moisture. Lower retrieval error associated with using multiple channels as compared to a single channel in soil moisture retrieval by statistical regression has been demonstrated. Existing algorithms for passive radiative transfer were shown to perform satisfactorily even though the vegetation cover was considerable. Vegetation plays a role in reducing the sensitivity of the PALS radar and radiometer and thereby increasing soil moisture retrieval error has been analyzed.

We observed good agreement between the radar- and radiometer-predicted soil moisture. The retrieved values of soil moisture tend to be overestimated which demonstrates the limitations of the change detection algorithm employed in this section, wherein the assumption that vegetation and roughness effects are present only as a bias in PALS active and passive observations are shown to be sources of error.

5.2. Use of Radar for Disaggregation of Passive Microwave Soil Moisture. In this section a simple algorithm for estimation of change in soil moisture at the spatial resolution of radar using low-resolution estimate of soil moisture from radiometer and copolarized backscattering coefficients has been proposed. The subpixel scale surface roughness variability does not play an important role in radar sensitivity to soil moisture at the L-band. Observations from combined radar/radiometer data from SMEX02, results from previous studies, and IEM simulations have been presented in support of this argument. Radar sensitivity to soil moisture at the L-band has been assumed to be a function of vegetation opacity only and further a simple soil moisture change estimation algorithm has been developed. Application of the algorithm to data

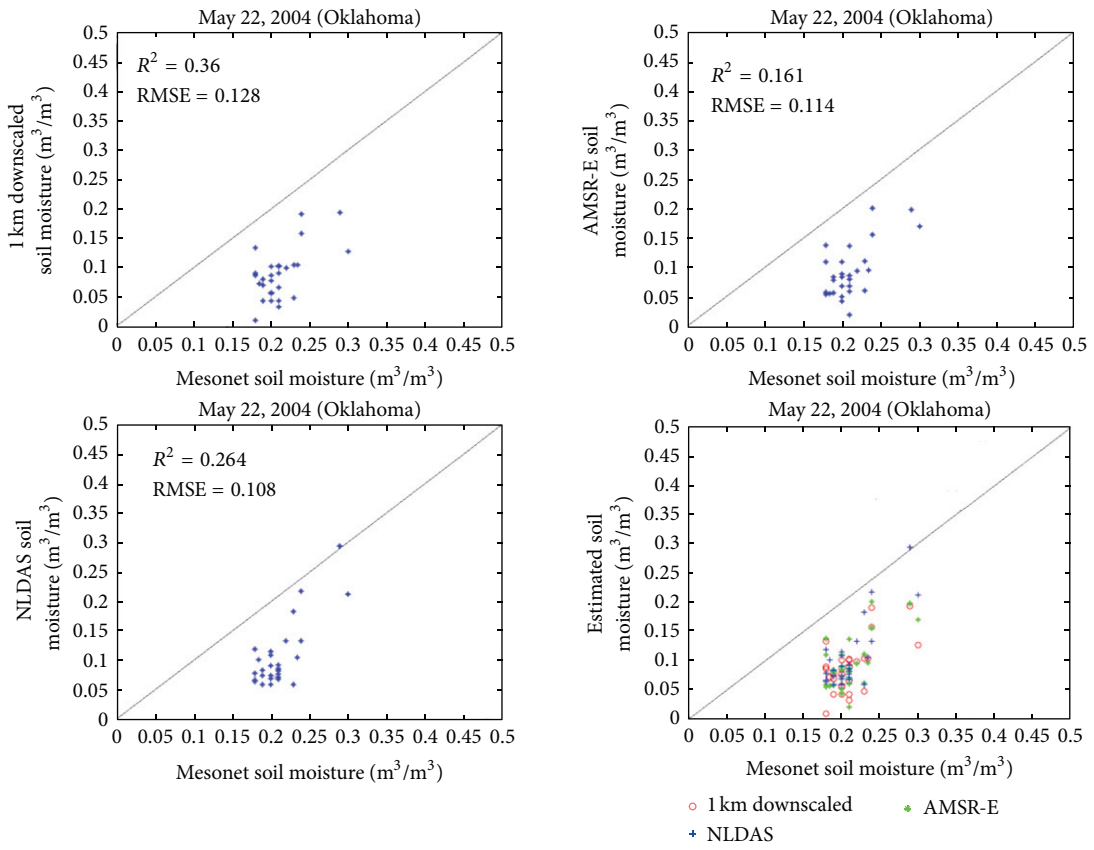

(a)

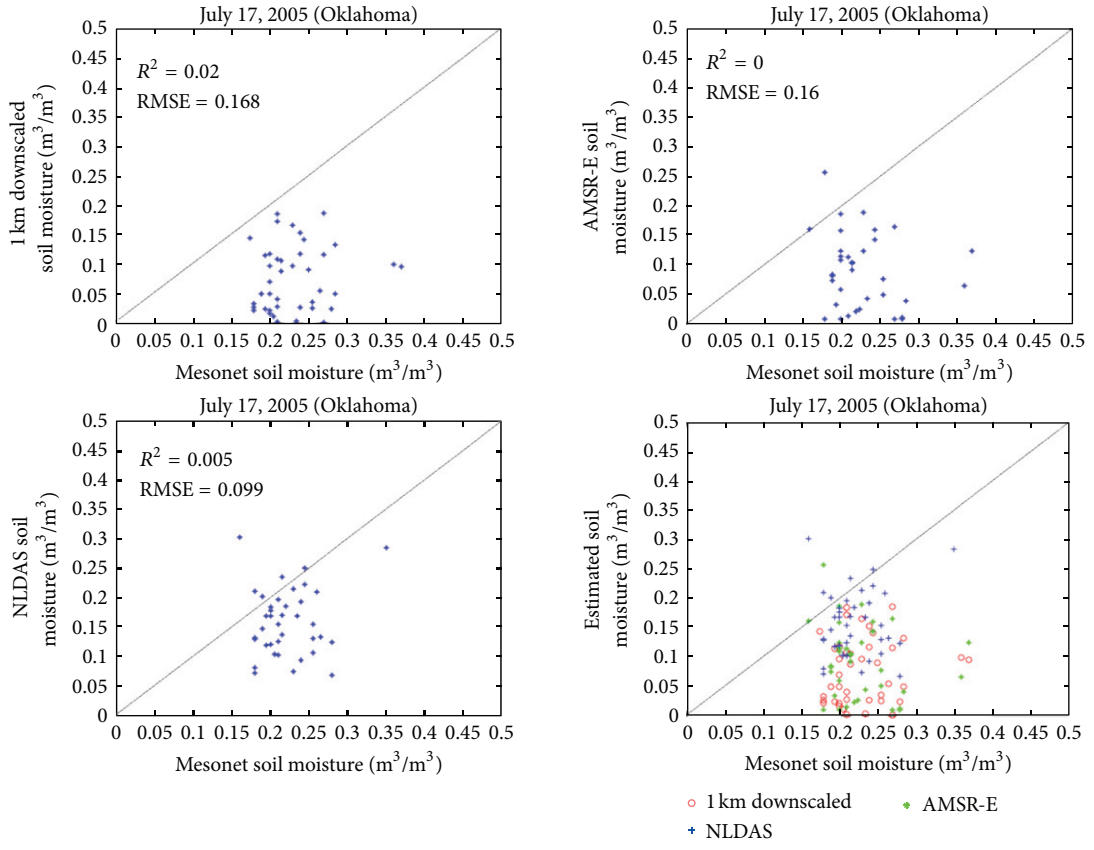

(b)

Figure 20: Continued.

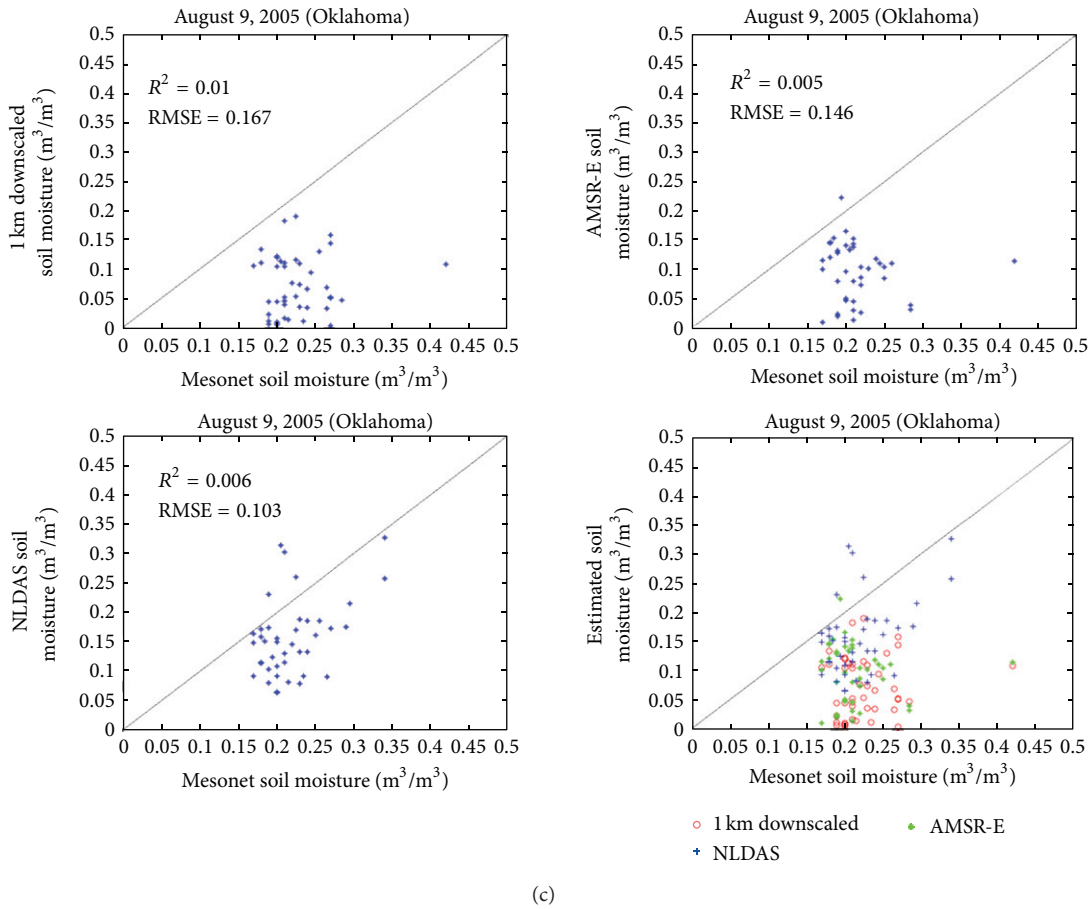

(c)

Figure 20: ((a)–(c)) Scatter plots of the 1 km, AMSR-E, and NLDAS soil moisture versus the Oklahoma Mesonet soil moisture observations for May 22, 2004, July 17, 2005, and August 9, 2005 [61].

obtained from the SMEX02 experiments results provided good results with root mean square error of prediction of 0.03 and 0.02 (error for estimated versus measured volumetric soil moisture, both at 100 m resolution) for two periods—July 5 to July 7 and July 7 to July 8. The R^2 value for both cases was 0.85.

The originality of the approach presented here lies in using radiometer to estimate soil moisture change at a lower spatial resolution (but with lower ancillary data requirements as compared to radar estimation of soil moisture) and then using change in radar backscatter to estimate the change in soil moisture at higher spatial resolution. The estimated change in soil moisture is a hydrologic variable of significant interest. A simple calibration methodology based on least error between modeled and measured soil moisture change values will allow a better estimation of parameters such as the hydraulic conductivity of soil layers. Mattikalli et al. reported that the 2-day soil moisture change was closely related to the saturated hydraulic conductivity (K_{sat}) profile [71]. It will be possible to relate K_{sat} from the radar/radiometer-algorithm-derived change in soil moisture with the added advantage of higher spatial resolution that will lead to more accurate estimation of water and energy fluxes. Future studies on the direction of radar/radiometer combination will have to aim at a better parameterization of the sensitivity relationship with vegetation opacity allowing the effect of vegetation heterogeneity to be addressed through the $f(\tau)$ parameter in the algorithm. Du et al., 2000, [117] have explored the behavior of soybean and grass canopies over medium rough surfaces. Their results indicate that it should be possible to develop simple parametric relationships between vegetation opacity and relative sensitivity. Estimation of vegetation opacity has been done in the past using optical sensors by estimation of vegetation water content using a proxy such as NDWI [83] and then using the empirical parameter b to relate vegetation opacity and water content [118]. This simple parameterization however has been shown to be too simple for canopies such as corn that are electrically thick scatterers and further research is required to find relationships between vegetation parameters and relative sensitivity over canopies such as corn. The approach presented in the paper should be applicable to data from the Hydros mission, at least over areas of low vegetation water content variability. The algorithm will have to be modified to account for vegetation variability within the radiometer footprint using the $f(\tau)$ parameter before it can be made operational.

5.3. Use of Near Infrared and Visible Data for Disaggregation of AMSR-E Soil Moisture. A soil moisture downscaling

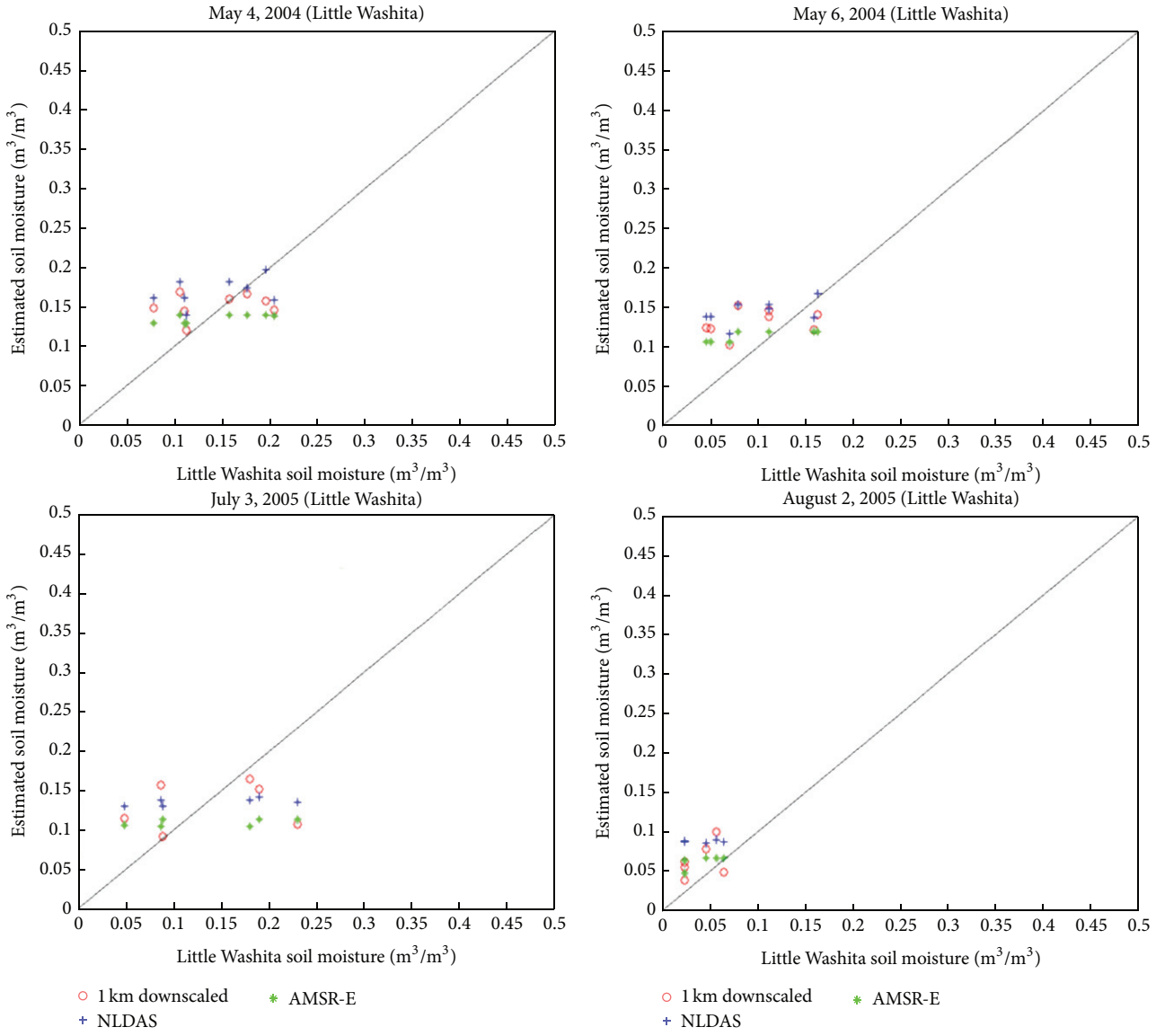

Figure 21: Scatter plot of the 1 km, AMSR-E, and NLDAS soil moisture versus the Oklahoma Mesonet soil moisture observations for May 4, 2004, May 6, 2004, July 3, 2005, and August 2, 2005 [61].

algorithm based on NLDAS-derived look-up curves that related daily surface temperature change and average daily soil moisture was developed. This algorithm was applied using MODIS products of clear days during crop growing seasons (May, July, and August of 2004~2005) in Oklahoma. Two sets of validation data, namely, Oklahoma Mesonet and Little Washita soil moisture observations, have been used to compare with the three estimates: 1 km downscaled soil moisture values, AMSR-E soil moisture values, and NLDAS soil moisture values. Statistical analyses and plots were used for analyzing accuracy of the downscaling algorithm.

Our results indicate the following. (a) The look-up regression curves support our assumption that the surface temperature change depends on the wetness of the land surface and that the vegetation modulates this relationship. (b) The 1 km downscaled maps provide details on the soil moisture spatial distribution patterns in Oklahoma as opposed to the AMSR-E maps. They also compare well with Oklahoma Mesonet soil moisture values. (c) The comparisons of all three datasets with the Oklahoma Mesonet soil moisture observations show an R^2 for the 1 km downscaled soil moisture ranging from 0.01~0.36, RMSE values ranging from 0.119~0.168 m^3/m^3, and standard deviation ranging from 0.043~0.058 m^3/m^3. The statistical comparisons show that the 1 km downscaled results correlate better to the Oklahoma Mesonet soil moisture observations than do AMSR-E and NLDAS soil moistures; (d) The statistical results for the 1 km downscaled soil moisture comparing with Little Washita Watershed soil moisture show good accuracy for the downscaling algorithm. Single-day comparisons showed RMSE values from 0.022~0.077 m^3/m^3,

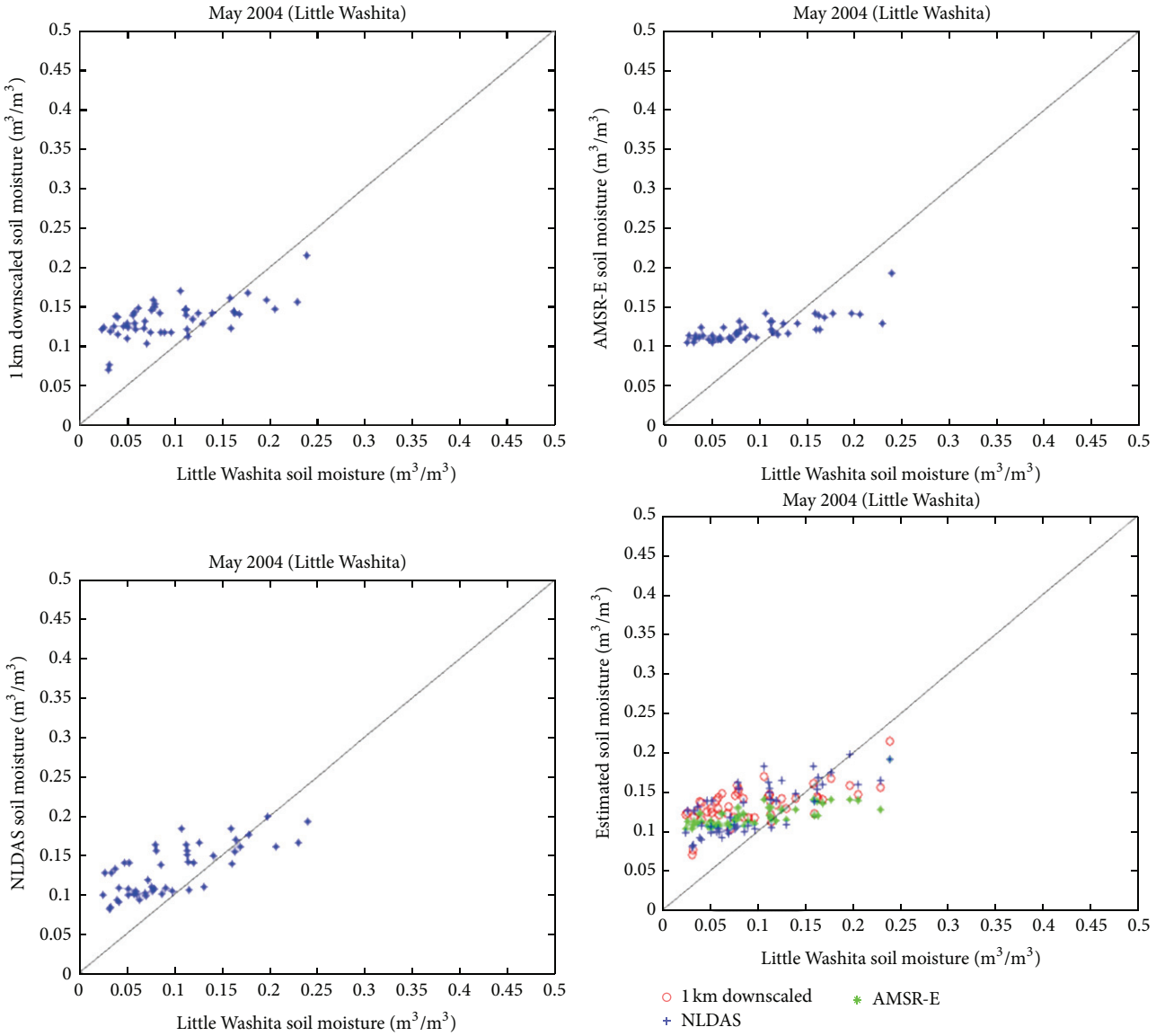

Figure 22: Scatter plot comparing AMSR-E, NLDAS, and 1 km downscaled soil moisture to the Little Washita soil moisture observations for all days of May 2004 [61].

standard deviations from <0.001~0.07 m^3/m^3, and bias values from −0.047~0.032 m^3/m^3. Taken as a whole for all of the clear days in May 2004, the R^2 and RMSE are 0.4 and 0.018 m^3/m^3, respectively. The errors between estimated and ground data used for validation for 1 km downscaled data are generally from −0.07~0.1 m^3/m^3, so the downscaled soil moisture has an error of 7%~36% of the total.

However, there are still several limitations that exist in this algorithm: (a) the MODIS temperature and NDVI products are often influenced by the cloud coverage; therefore this method is not an all-weather algorithm for downscaling, (b) the accuracy of the AMSR-E and NLDAS soil moisture determines the accuracy of the 1 km downscaled soil moisture, and (c) Only vegetation and temperature were used in developing this downscaling algorithm, and the high spatial resolution data of these variables would be required. This methodology is based on preserving the 25 km mean soil moisture same as the AMSR-E soil moisture estimates. So, any overall day-to-day bias present in the AMSR-E soil moisture retrievals will be present in the disaggregated 1 km estimates. But if we compare our results with those reported in the literature and presented in Section 1 and Table 1 we note that this analysis included a large area (the entire state of Oklahoma) and a moderate period of time as opposed to some previous studies, which only included shorter-term field experiments or smaller catchments. However, our correlations values for R^2 do compare well with the values noted in these studies [50] of 0.14–0.21; the RMSE shows similar favorable comparisons.

Future work that will combine this approach with our previous active-passive downscaling approach [55] is being pursued and this will offer much better progress in downscaling of soil moisture for catchment studies.

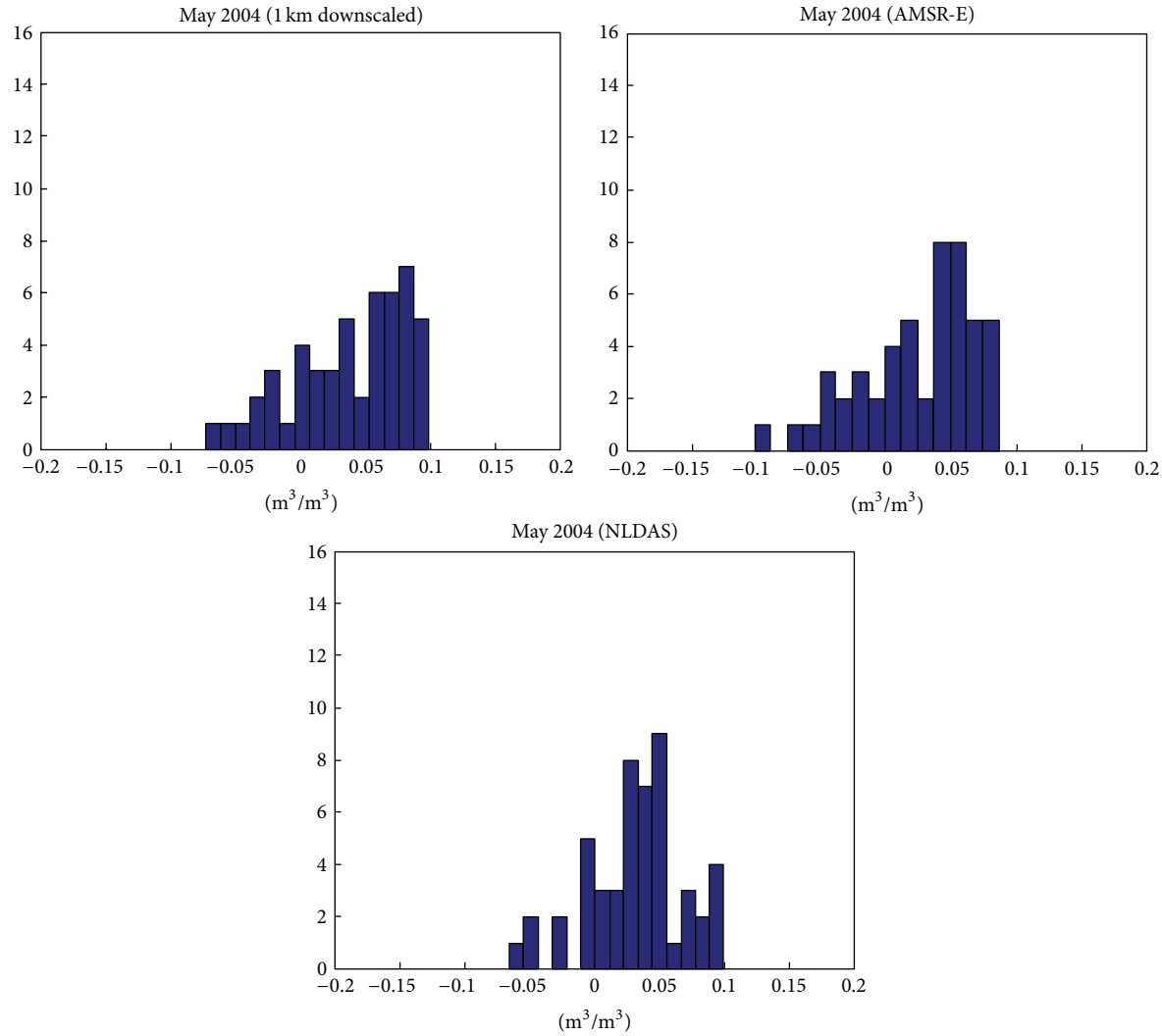

Figure 23: Frequency distribution of difference between the 1 km, AMSR-E, and NLDAS estimates of soil moisture and the Little Washita soil moisture observations for May 2004 [61].

References

[1] K. L. Brubaker and D. Entekhabi, "Analysis of feedback mechanisms in land-atmosphere interaction," *Water Resources Research*, vol. 32, no. 5, pp. 1343–1357, 1996.

[2] T. Delworth and S. Manabe, "The influence of soil wetness on near-surface atmospheric variability," *Journal of Climate*, vol. 2, pp. 1447–1462, 1989.

[3] R. A. Pielke, "Influence of the spatial distribution of vegetation and soils on the prediction of cumulus convective rainfall," *Reviews of Geophysics*, vol. 39, no. 2, pp. 151–177, 2001.

[4] J. Shukla and Y. Mintz, "Influence of land-surface evapotranspiration on the earth's climate," *Science*, vol. 215, no. 4539, pp. 1498–1501, 1982.

[5] Jy-Tai Chang and P. J. Wetzel, "Effects of spatial variations of soil moisture and vegetation on the evolution of a prestorm environment: a numerical case study," *Monthly Weather Review*, vol. 119, no. 6, pp. 1368–1390, 1991.

[6] E. Engman, "Soil moisture, the hydrologic interface between surface and ground waters," in *Remote Sensing and Geographic Information Systems for Design and Operation of Water Resources Systems*, International Association of Hydrological Sciences no. 242, 1997.

[7] J. Mahfouf, E. Richard, and P. Mascarat, "The influence of soil and vegetation on Mesoscale circulations," *Journal of Climate and Applied Climatology*, vol. 26, pp. 1483–1495, 1987.

[8] J. Laccini, T. Carlson, and T. Warner, "Sensitivity of the Great Plains severe storm environment to soil moisture distribution," *Monthly Weather Review*, vol. 115, pp. 2660–2673, 1987.

[9] D. Zhang and R. A. Anthes, "A high-resolution model of the planetary boundary layer—sensitivity tests and comparisons with SESAME-79 data," *Journal of Applied Meteorology*, vol. 21, no. 11, pp. 1594–1609, 1982.

[10] P. R. Houser, W. J. Shuttleworth, J. S. Famiglietti, H. V. Gupta, K. H. Syed, and D. C. Goodrich, "Integration of soil moisture remote sensing and hydrologic modeling using data assimilation," *Water Resources Research*, vol. 34, no. 12, pp. 3405–3420, 1998.

[11] S. Zhang, H. Li, W. Zhang, C. Qiu, and X. Li, "Estimating the soil moisture profile by assimilating near-surface observations with the ensemble Kalman Filter (EnKF)," *Advances in Atmospheric Sciences*, vol. 22, no. 6, pp. 936–945, 2005.

[12] W. Ni-Meister, P. R. Houser, and J. P. Walker, "Soil moisture initialization for climate prediction: assimilation of scanning multifrequency microwave radiometer soil moisture data into a land surface model," *Journal of Geophysical Research D*, vol. 111, no. 20, Article ID D20102, 2006.

[13] J. P. Hollinger, J. L. Pierce, and G. A. Poe, "SSM/I instrument evaluation," *IEEE Transactions on Geoscience and Remote Sensing*, vol. 28, no. 5, pp. 781–790, 1990.

[14] E. Njoku, B. Rague, and K. Fleming, *The Nimbus-7 SMMR Pathfinder Brightness Data Set*, Jet Propulsion Lab, Pasadena, Calif, USA, 1998.

[15] S. Paloscia, G. Macelloni, E. Santi, and T. Koike, "A multifrequency algorithm for the retrieval of soil moisture on a large scale using microwave data from SMMR and SSM/I satellites," *IEEE Transactions on Geoscience and Remote Sensing*, vol. 39, no. 8, pp. 1655–1661, 2001.

[16] A. Guha and V. Lakshmi, "Sensitivity, spatial heterogeneity, and scaling of C-band microwave brightness temperatures for land hydrology studies," *IEEE Transactions on Geoscience and Remote Sensing*, vol. 40, no. 12, pp. 2626–2635, 2002.

[17] A. Guha and V. Lakshmi, "Use of the Scanning Multichannel Microwave Radiometer (SMMR) to retrieve soil moisture and surface temperature over the central United States," *IEEE Transactions on Geoscience and Remote Sensing*, vol. 42, no. 7, pp. 1482–1494, 2004.

[18] J. Wen, T. J. Jackson, R. Bindlish, A. Y. Hsu, and Z. B. Su, "Retrieval of soil moisture and vegetation water content using SSM/I data over a corn and soybean region," *Journal of Hydrometeorology*, vol. 6, no. 6, pp. 854–863, 2005.

[19] V. Lakshmi, "Special sensor microwave imager data in field experiments: FIFE-1987," *International Journal of Remote Sensing*, vol. 19, no. 3, pp. 481–505, 1998.

[20] V. Lakshmi, E. F. Wood, and B. J. Choudhury, "A soil-canopy-atmosphere model for use in satellite microwave remote sensing," *Journal of Geophysical Research D*, vol. 102, no. 6, pp. 6911–6927, 1997.

[21] V. Lakshmi, E. F. Wood, and B. J. Choudhury, "Investigation of effect of heterogeneities in vegetation and rainfall on simulated SSM/I brightness temperatures," *International Journal of Remote Sensing*, vol. 18, no. 13, pp. 2763–2784, 1997.

[22] V. Lakshmi, E. F. Wood, and B. J. Choudhury, "Evaluation of Special Sensor Microwave/Imager satellite data for regional soil moisture estimation over the Red River basin," *Journal of Applied Meteorology*, vol. 36, no. 10, pp. 1309–1328, 1997.

[23] L. Li, P. Gaiser, T. J. Jackson, R. Bindlish, and J. Du, "WindSat soil moisture algorithm and validation," in *Proceedings of the International Geoscience and Remote Sensing Symposium*, pp. 1188–1191, Barcelona, Spain, July 2007.

[24] H. Gao, E. F. Wood, T. J. Jackson, M. Drusch, and R. Bindlish, "Using TRMM/TMI to retrieve surface soil moisture over the southern United States from 1998 to 2002," *Journal of Hydrometeorology*, vol. 7, no. 1, pp. 23–38, 2006.

[25] M. Owe, R. de Jeu, and T. Holmes, "Multisensor historical climatology of satellite-derived global land surface moisture," *Journal of Geophysical Research F*, vol. 113, no. 1, Article ID F01002, 2008.

[26] W. Wagner, V. Naeimi, K. Scipal, R. Jeu, and J. Martínez-Fernández, "Soil moisture from operational meteorological satellites," *Hydrogeology Journal*, vol. 15, no. 1, pp. 121–131, 2007.

[27] C. Rüdiger, J. C. Calvet, C. Gruhier, T. R. H. Holmes, R. A. M. de Jeu, and W. Wagner, "An intercomparison of ERS-Scat and AMSR-E soil moisture observations with model simulations over France," *Journal of Hydrometeorology*, vol. 10, no. 2, pp. 431–447, 2009.

[28] C. S. Draper, J. P. Walker, P. J. Steinle, R. A. M. de Jeu, and T. R. H. Holmes, "An evaluation of AMSR-E derived soil moisture over Australia," *Remote Sensing of Environment*, vol. 113, no. 4, pp. 703–710, 2009.

[29] R. A. M. Jeu, W. Wagner, T. R. H. Holmes, A. J. Dolman, N. C. Giesen, and J. Friesen, "Global soil moisture patterns observed by space borne microwave radiometers and scatterometers," *Surveys in Geophysics*, vol. 29, no. 4-5, pp. 399–420, 2008.

[30] K. Imaoka, M. Kachi, H. Fujii et al., "Global change observation mission (GCOM) for monitoring carbon, water cycles, and climate change," *Proceedings of the IEEE*, vol. 98, no. 5, pp. 717–734, 2010.

[31] E. G. Njoku and D. Entekhabi, "Passive microwave remote sensing of soil moisture," *Journal of Hydrology*, vol. 184, no. 1-2, pp. 101–129, 1996.

[32] F. T. Ulaby, P. C. Dubois, and J. Van Zyl, "Radar mapping of surface soil moisture," *Journal of Hydrology*, vol. 184, no. 1-2, pp. 57–84, 1996.

[33] T. J. Schmugge, W. P. Kustas, J. C. Ritchie, T. J. Jackson, and A. Rango, "Remote sensing in hydrology," *Advances in Water Resources*, vol. 25, no. 8-12, pp. 1367–1385, 2002.

[34] F. T. Ulaby, M. Razani, and M. C. Dobson, "Effect of vegetation cover on the microwave radiometric sensitivity to soil moisture," *IEEE Transactions on Geoscience and Remote Sensing*, vol. 21, no. 1, pp. 51–61, 1983.

[35] B. J. Choudhury, T. J. Schmugge, R. W. Newton, and A. Chang, "Effect of surface roughness on the microwave emission from soils," *Journal of Geophysical Research*, vol. 89, no. 9, pp. 5699–5706, 1979.

[36] F. Ulaby, R. K. Moore, and A. K. Fung, *Microwave Remote Sensing: Active and Passive, Vol. III—Volume Scattering and Emission Theory, Advanced Systems and Applications*, Artech House, Dedham, Mass, USA, 1986.

[37] J. R. Wang, J. C. Shiue, T. J. Schmugge, and E. T. Engman, "The L-band PBMR measurements of surface soil moisture in FIFE," *IEEE Transactions on Geoscience and Remote Sensing*, vol. 28, no. 5, pp. 906–914, 1990.

[38] T. Schmugge, T. J. Jackson, W. P. Kustas, and J. R. Wang, "Passive microwave remote sensing of soil moisture: results from HAPEX, FIFE and MONSOON' 90," *ISPRS Journal of Photogrammetry and Remote Sensing*, vol. 47, no. 2-3, pp. 127–143, 1992.

[39] P. E. O'Neill, N. S. Chauhan, and T. J. Jackson, "Use of active and passive microwave remote sensing for soil moisture estimation through corn," *International Journal of Remote Sensing*, vol. 17, no. 10, pp. 1851–1865, 1996.

[40] J. D. Bolten, V. Lakshmi, and E. G. Njoku, "A passive-active retrieval of soil moisture for the Southern great plains 1999 experiment," *IEEE Transactions on Geoscience and Remote Sensing*, vol. 41, no. 12, pp. 2792–2801, 2003.

[41] U. Narayan, V. Lakshmi, and E. G. Njoku, "Retrieval of soil moisture from passive and active L/S band sensor (PALS) observations during the Soil Moisture Experiment in 2002 (SMEX02)," *Remote Sensing of Environment*, vol. 92, no. 4, pp. 483–496, 2004.

[42] E. G. Njoku, W. J. Wilson, S. H. Yueh et al., "Observations of soil moisture using a passive and active low-frequency microwave airborne sensor during SGP99," *IEEE Transactions on Geoscience and Remote Sensing*, vol. 40, no. 12, pp. 2659–2673, 2002.

[43] F. Brock, K. Crawford, R. L. Elliott et al., "The oklahoma mesonet—a technical overview," *Journal of Atmospheric and Oceanic Technology*, vol. 12, no. 1, pp. 5–19, 1995.

[44] B. G. Illston, J. B. Basara, and K. C. Crawford, "Seasonal to interannual variations of soil moisture measured in Oklahoma," *International Journal of Climatology*, vol. 24, no. 15, pp. 1883–1896, 2004.

[45] B. G. Illston, J. B. Basara, D. K. Fisher et al., "Mesoscale monitoring of soil moisture across a statewide network," *Journal of Atmospheric and Oceanic Technology*, vol. 25, no. 2, pp. 167–182, 2008.

[46] S. E. Hollinger and S. A. Isard, "A soil moisture climatology of Illinois," *Journal of Climate*, vol. 7, no. 5, pp. 822–833, 1994.

[47] G. L. Schaefer, M. H. Cosh, and T. J. Jackson, "The USDA natural resources conservation service soil climate analysis network (SCAN)," *Journal of Atmospheric and Oceanic Technology*, vol. 24, no. 12, pp. 2073–2077, 2007.

[48] G. C. Heathman, M. H. Cosh, E. Han, T. J. Jackson, L. G. McKee, and S. McAfee, "Field scale spatiotemporal analysis of surface soil moisture for evaluating point-scale in situ networks," *Geoderma*, vol. 170, pp. 195–205, 2012.

[49] O. Merlin, A. Al Bitar, J. P. Walker, and Y. Kerr, "An improved algorithm for disaggregating microwave-derived soil moisture based on red, near-infrared and thermal-infrared data," *Remote Sensing of Environment*, vol. 114, no. 10, pp. 2305–2316, 2010.

[50] M. Piles, A. Camps, M. Vall-llossera et al., "Downscaling SMOS-derived soil moisture using MODIS visible/infrared data," *IEEE Transactions on Geoscience and Remote Sensing*, vol. 49, no. 9, pp. 3156–3166, 2011.

[51] O. Merlin, A. Chehbouni, J. P. Walker, R. Panciera, and Y. H. Kerr, "A simple method to disaggregate passive microwave-based soil moisture," *IEEE Transactions on Geoscience and Remote Sensing*, vol. 46, no. 3, pp. 786–796, 2008.

[52] O. Merlin, A. Al Bitar, J. P. Walker, and Y. Kerr, "A sequential model for disaggregating near-surface soil moisture observations using multi-resolution thermal sensors," *Remote Sensing of Environment*, vol. 113, no. 10, pp. 2275–2284, 2009.

[53] D. Entekhabi, E. G. Njoku, P. E. O'Neill et al., "The soil moisture active passive (SMAP) mission," *Proceedings of the IEEE*, vol. 98, no. 5, pp. 704–716, 2010.

[54] T. Schmugge, P. Gloersen, T. Wilheit, and F. Geiger, "Remote sensing of soil moisture with microwave radiometers," *Journal of Geophysical Research*, vol. 79, no. 2, pp. 317–323, 1974.

[55] U. Narayan, V. Lakshmi, and T. J. Jackson, "High-resolution change estimation of soil moisture using L-band radiometer and radar observations made during the SMEX02 experiments," *IEEE Transactions on Geoscience and Remote Sensing*, vol. 44, no. 6, pp. 1545–1554, 2006.

[56] U. Narayan and V. Lakshmi, "Characterizing subpixel variability of low resolution radiometer derived soil moisture using high resolution radar data," *Water Resources Research*, vol. 44, no. 6, Article ID W06425, 2008.

[57] N. N. Das, D. Entekhabi, and E. G. Njoku, "An algorithm for merging SMAP radiometer and radar data for high-resolution soil-moisture retrieval," *IEEE Transactions on Geoscience and Remote Sensing*, vol. 49, no. 5, pp. 1504–1512, 2011.

[58] O. Merlin, A. Al Bitar, V. Rivalland, P. Béziat, E. Ceschia, and G. Dedieu, "An analytical model of evaporation efficiency for unsaturated soil surfaces with an arbitrary thickness," *Journal of Applied Meteorology and Climatology*, vol. 50, no. 2, pp. 457–471, 2011.

[59] O. Merlin, F. Jacob, J.-P. Wigneron et al., "Multidimensional disaggregation of land surface temperature using high-resolution red, near-infrared, shortwave-infrared, and microwave-L bands," *IEEE Transactions on Geoscience and Remote Sensing*, vol. 50, no. 5, pp. 1864–1880, 2012.

[60] O. Merlin, C. Rudiger, A. Al Bitar et al., "Disaggregation of SMOS soil moisture in Southeastern Australia," *IEEE Transactions on Geoscience and Remote Sensing*, vol. 50, no. 5, pp. 1556–1571, 2012.

[61] B. Fang, V. Lakshmi, R. Bindlish, T. Jackson, M. Cosh, and J. Basara, "Passive microwave soil moisture downscaling using vegetation and surface temperature," *Vadose Zone Journal*. In review.

[62] M. A. Friedl, D. K. McIver, J. C. F. Hodges et al., "Global land cover mapping from MODIS: algorithms and early results," *Remote Sensing of Environment*, vol. 83, no. 1-2, pp. 287–302, 2002.

[63] J. R. Wang and T. J. Schmugge, "An empirical model for the complex dielectric permittivity of soils as a function of water content," *IEEE Transactions on Geoscience and Remote Sensing*, vol. GE-18, no. 4, pp. 288–295, 1980.

[64] M. C. Dobson, F. T. Ulaby, M. T. Hallikainen, and M. A. El-Rayes, "Microwave dielectric behavior of wet soil—part 2: dielectric mixing models," *IEEE Transactions on Geoscience and Remote Sensing*, vol. GE-23, no. 1, pp. 35–46, 1985.

[65] A. K. Fung, Z. Li, and K. S. Chen, "Backscattering from a randomly rough dielectric surface," *IEEE Transactions on Geoscience and Remote Sensing*, vol. 30, no. 2, pp. 356–369, 1992.

[66] T. Schmugge, "Remote sensing of soil moisture," in *Hydrological Forecasting*, M. G. Anderson and T. P. Burt, Eds., John Wiley & Sons, New York, NY, USA, 1985.

[67] R. R. Gillies and T. N. Carlson, "Thermal remote sensing of surface soil water content with partial vegetation cover for incorporation into climate models," *Journal of Applied Meteorology*, vol. 34, no. 4, pp. 745–756, 1995.

[68] S. J. Goetz, "Multi-sensor analysis of NDVI, surface temperature and biophysical variables at a mixed grassland site," *International Journal of Remote Sensing*, vol. 18, no. 1, pp. 71–94, 1997.

[69] T. Mo, B. J. Choudhury, T. J. Schmugge, J. R. Wang, and T. J. Jackson, "A model for the microwave emission from vegetation covered fields," *Journal of Geophysical Research*, vol. 87, pp. 11 229–11 237, 1982.

[70] E. T. Engman and N. Chauhan, "Status of microwave soil moisture measurements with remote sensing," *Remote Sensing of Environment*, vol. 51, no. 1, pp. 189–198, 1995.

[71] N. M. Mattikalli, E. T. Engman, L. R. Ahuja, and T. J. Jackson, "Microwave remote sensing of soil moisture for estimation of profile soil property," *International Journal of Remote Sensing*, vol. 19, no. 9, pp. 1751–1767, 1998.

[72] C. A. Laymon, W. L. Crosson, V. V. Soman et al., "Huntsville '98: an expirement in ground-based microwave remote sensing of soil moisture," *International Journal of Remote Sensing*, vol. 20, no. 2–4, pp. 823–828, 1999.

[73] E. G. Njoku and L. Li, "Retrieval of land surface parameters using passive microwave measurements at 6-18 GHz," *IEEE Transactions on Geoscience and Remote Sensing*, vol. 37, no. 1, pp. 79–93, 1999.

[74] Y. H. Kerr and E. G. Njoku, "Semiempirical model for interpreting microwave emission from semiarid land surfaces as seen from space," *IEEE Transactions on Geoscience and Remote Sensing*, vol. 28, no. 3, pp. 384–393, 1990.

[75] Y. Oh, K. Sarabandi, and F. T. Ulaby, "An empirical model and an inversion technique for radar scattering from bare soil surfaces," *IEEE Transactions on Geoscience and Remote Sensing*, vol. 30, no. 2, pp. 370–381, 1992.

[76] P. C. Dubois, J. van Zyl, and T. Engman, "Measuring soil moisture with imaging radars," *IEEE Transactions on Geoscience and Remote Sensing*, vol. 33, no. 4, pp. 915–926, 1995.

[77] J. Shi, J. Wang, A. Y. Hsu, P. E. O'Neill, and E. T. Engman, "Estimation of bare surface soil moisture and surface roughness parameter using L-band SAR image data," *IEEE Transactions on Geoscience and Remote Sensing*, vol. 35, no. 5, pp. 1254–1266, 1997.

[78] T. J. Jackson, J. Schmugge, and E. T. Engman, "Remote sensing applications to hydrology: soil moisture," *Hydrological Sciences Journal*, vol. 41, no. 4, pp. 517–530, 1996.

[79] M. Owe, A. A. Van De Griend, R. De Jeu, J. J. De Vries, E. Seyhan, and E. T. Engman, "Estimating soil moisture from satellite microwave observations: past and ongoing projects, and relevance to GCIP," *Journal of Geophysical Research D*, vol. 104, no. 16, pp. 19735–19742, 1999.

[80] J. D. Villasenor, D. R. Fatland, and L. D. Hinzman, "Change detection on Alaska's North Slope using repeat-pass ERS-1 SAR images," *IEEE Transactions on Geoscience and Remote Sensing*, vol. 31, no. 1, pp. 227–236, 1993.

[81] M. C. Dobson and F. T. Ulaby, "Active microwave soil-moisture research," *IEEE Transactions on Geoscience and Remote Sensing*, vol. 24, no. 1, pp. 23–36, 1986.

[82] M. C. Dobson and F. T. Ulaby, "Preliminary evaluation of the Sir-B response to soil-moisture, surface-roughness, and crop canopy cover," *IEEE Transactions on Geoscience and Remote Sensing*, vol. 24, no. 4, pp. 517–526, 1986.

[83] T. J. Jackson, D. Chen, M. Cosh et al., "Vegetation water content mapping using Landsat data derived normalized difference water index for corn and soybeans," *Remote Sensing of Environment*, vol. 92, no. 4, pp. 475–482, 2004.

[84] M. H. Cosh, T. J. Jackson, R. Bindlish, and J. H. Prueger, "Watershed scale temporal and spatial stability of soil moisture and its role in validating satellite estimates," *Remote Sensing of Environment*, vol. 92, no. 4, pp. 427–435, 2004.

[85] A. S. Limaye, W. L. Crosson, C. A. Laymon, and E. G. Njoku, "Land cover-based optimal deconvolution of PALS L-band microwave brightness temperatures," *Remote Sensing of Environment*, vol. 92, no. 4, pp. 497–506, 2004.

[86] L. Yunling, K. Yunjin, and J. van Zyl, "The NASA/JPL airborne synthetic aperture radar system," 2002, http://airsar.jpl.nasa.gov/documents/genairsar/airsar_paper1.pdf.

[87] K. Mallick, B. K. Bhattacharya, and N. K. Patel, "Estimating volumetric surface moisture content for cropped soils using a soil wetness index based on surface temperature and NDVI," *Agricultural and Forest Meteorology*, vol. 149, no. 8, pp. 1327–1342, 2009.

[88] I. Sandholt, K. Rasmussen, and J. Andersen, "A simple interpretation of the surface temperature/vegetation index space for assessment of surface moisture status," *Remote Sensing of Environment*, vol. 79, no. 2-3, pp. 213–224, 2002.

[89] T. N. Carlson, R. R. Gillies, and T. J. Schmugge, "An interpretation of methodologies for indirect measurement of soil water content," *Agricultural and Forest Meteorology*, vol. 77, no. 3-4, pp. 191–205, 1995.

[90] T. N. Carlson and D. A. Ripley, "On the relation between NDVI, fractional vegetation cover, and leaf area index," *Remote Sensing of Environment*, vol. 62, no. 3, pp. 241–252, 1997.

[91] M. Minacapilli, M. Iovino, and F. Blanda, "High resolution remote estimation of soil surface water content by a thermal inertia approach," *Journal of Hydrology*, vol. 379, no. 3-4, pp. 229–238, 2009.

[92] T. R. Karl, G. Kukla, and J. Gavin, "Decreasing diurnal temperature range in the United States and Canada from 1941 through 1980," *Journal of Climate & Applied Meteorology*, vol. 23, no. 11, pp. 1489–1504, 1984.

[93] G. J. Collatz, L. Bounoua, S. O. Los, D. A. Randall, I. Y. Fung, and P. J. Sellers, "A mechanism for the influence of vegetation on the response of the diurnal temperature range to changing climate," *Geophysical Research Letters*, vol. 27, no. 20, pp. 3381–3384, 2000.

[94] A. Dai and C. Deser, "Diurnal and semidiurnal variations in global surface wind and divergence fields," *Journal of Geophysical Research D*, vol. 104, no. 24, pp. 31109–31125, 1999.

[95] T. J. Jackson, D. M. Le Vine, A. Y. Hsu et al., "Soil moisture mapping at regional scales using microwave radiometry: the Southern great plains hydrology experiment," *IEEE Transactions on Geoscience and Remote Sensing*, vol. 37, no. 5, pp. 2136–2151, 1999.

[96] T. J. Jackson, A. J. Gasiewski, A. Oldak et al., "Soil moisture retrieval using the C-band polarimetric scanning radiometer during the Southern Great Plains 1999 Experiment," *IEEE Transactions on Geoscience and Remote Sensing*, vol. 40, no. 10, pp. 2151–2161, 2002.

[97] T. J. Jackson, M. H. Cosh, R. Bindlish et al., "Validation of advanced microwave scanning radiometer soil moisture products," *IEEE Transactions on Geoscience and Remote Sensing*, vol. 48, no. 12, pp. 4256–4272, 2010.

[98] I. Mladenova, V. Lakshmi, T. J. Jackson, J. P. Walker, O. Merlin, and R. A. M. de Jeu, "Validation of AMSR-E soil moisture using L-band airborne radiometer data from National Airborne Field Experiment 2006," *Remote Sensing of Environment*, vol. 115, no. 8, pp. 2096–2103, 2011.

[99] K. E. Mitchell, D. Lohmann, P. R. Houser et al., "The multi-institution North American Land Data Assimilation System (NLDAS): utilizing multiple GCIP products and partners in a continental distributed hydrological modeling system," *Journal of Geophysical Research D*, vol. 109, no. D7, article D07, 2004.

[100] B. A. Cosgrove, D. Lohmann, K. E. Mitchell et al., "Real-time and retrospective forcing in the North American Land Data Assimilation System (NLDAS) project," *Journal of Geophysical Research D*, vol. 108, no. 22, pp. 1–12, 2003.

[101] D. Lohmann, K. E. Mitchell, P. R. Houser et al., "Streamflow and water balance intercomparisons of four land surface models in the North American Land Data Assimilation Project," *Journal of Geophysical Research*, vol. 109, Article ID D07S91, 2004.

[102] D. Lohmann, K. E. Mitchell, P. R. Houser et al., "Streamflow and water balance intercomparisons of four land surface models in the North American Land Data Assimilation System project," *Journal of Geophysical Research D*, vol. 109, no. 7, Article ID D07S91, 2004.

[103] A. Robock, L. Luo, E. F. Wood et al., "Evaluation of the North American Land Data Assimilation System over the Southern Great Pkains during the warm season," *Journal of Geophysical Research*, vol. 108, no. D22, article 8846, 2003.

[104] J. C. Schaake, Q. Duan, V. Koren et al., "An intercomparison of soil moisture fields in the North American Land Data Assimilation System (NLDAS)," *Journal of Geophysical Research D*, vol. 109, no. 1, Article ID D01S90, 2004.

[105] E. G. Njoku, T. J. Jackson, V. Lakshmi, T. K. Chan, and S. V. Nghiem, "Soil moisture retrieval from AMSR-E," *IEEE*

Transactions on Geoscience and Remote Sensing, vol. 41, no. 2, pp. 215–229, 2003.

[106] E. G. Njoku and S. K. Chan, "Vegetation and surface roughness effects on AMSR-E land observations," *Remote Sensing of Environment*, vol. 100, no. 2, pp. 190–199, 2006.

[107] T. J. Jackson, "III. Measuring surface soil moisture using passive microwave remote sensing," *Hydrological Processes*, vol. 7, no. 2, pp. 139–152, 1993.

[108] C. O. Justice, J. R. G. Townshend, E. F. Vermote et al., "An overview of MODIS Land data processing and product status," *Remote Sensing of Environment*, vol. 83, no. 1-2, pp. 3–15, 2002.

[109] C. J. Tucker, "Red and photographic infrared linear combinations for monitoring vegetation," *Remote Sensing of Environment*, vol. 8, no. 2, pp. 127–150, 1979.

[110] R. B. Myneni, F. G. Hall, P. J. Sellers, and A. L. Marshak, "Interpretation of spectral vegetation indexes," *IEEE Transactions on Geoscience and Remote Sensing*, vol. 33, no. 2, pp. 481–486, 1995.

[111] R. B. Myneni, S. Hoffman, Y. Knyazikhin et al., "Global products of vegetation leaf area and fraction absorbed PAR from year one of MODIS data," *Remote Sensing of Environment*, vol. 83, no. 1-2, pp. 214–231, 2002.

[112] R. S. De Fries, M. Hansen, J. R. G. Townshend, and R. Sohlberg, "Global land cover classifications at 8 km spatial resolution: the use of training data derived from Landsat imagery in decision tree classifiers," *International Journal of Remote Sensing*, vol. 19, no. 16, pp. 3141–3168, 1998.

[113] Z. Wan and Z. L. Li, "A physics-based algorithm for retrieving land-surface emissivity and temperature from EOS/MODIS data," *IEEE Transactions on Geoscience and Remote Sensing*, vol. 35, no. 4, pp. 980–996, 1997.

[114] R. A. McPherson, C. A. Fiebrich, K. C. Crawford et al., "Statewide monitoring of the mesoscale environment: a technical update on the Oklahoma Mesonet," *Journal of Atmospheric and Oceanic Technology*, vol. 24, no. 3, pp. 301–321, 2007.

[115] J. L. Heilman and D. G. Moore, "Evaluating near-surface soil moisture using heat capacity mapping mission data," *Remote Sensing of Environment*, vol. 12, no. 2, pp. 117–121, 1982.

[116] S. Hong, V. Lakshmi, E. E. Small, and F. Chen, "The influence of the land surface on hydrometeorology and ecology: new advances from modeling and satellite remote sensing," *Hydrology Research*, vol. 42, no. 2-3, pp. 95–112, 2011.

[117] Y. Du, F. T. Ulaby, and M. C. Dobson, "Sensitivity to soil moisture by active and passive microwave sensors," *IEEE Transactions on Geoscience and Remote Sensing*, vol. 38, no. 1, pp. 105–114, 2000.

[118] T. J. Jackson and T. J. Schmugge, "Vegetation effects on the microwave emission of soils," *Remote Sensing of Environment*, vol. 36, no. 3, pp. 203–212, 1991.